LOW TEMPERATURE ELECTROCATALYTIC REDUCTION OF CARBON DIOXIDE UTILIZING ROOM TEMPERATURE IONIC LIQUIDS

BY

BRIAN A. ROSEN

THESIS

Submitted in partial fulfillment of the requirements
for the degree of Master of Science in Chemical Engineering
in the Graduate College of the
University of Illinois at Urbana-Champaign, 2010

Urbana, Illinois

Adviser:

Professor Richard I. Masel

ABSTRACT

Artificial photosynthesis, where one uses electricity from solar, or wind, to convert water and carbon dioxide into a hydrocarbon fuel could provide a viable route to renewable fuels but so far the results have been stymied because of the lack of a CO_2 conversion catalyst that operates at low overpotentials. In this study we report a catalyst system that shows CO_2 conversion at low overpotentials. The system uses two different catalysts to achieve the conversion. First an ionic liquid or ionic salt is used to catalyze the formation of a $(CO_2)^-$ intermediate. Then a transition metal is used to catalyze the conversion of the $(CO_2)^-$ intermediate into useful products. CO formation is first observed at -250mV with respect to a standard hydrogen electrode compared to -800mV in the absence of the ionic liquid. Thus, CO_2 conversion to CO can occur without the large energy loss associated with a high overpotential raising the possibility of practical artificial photosynthesis. The reduction of CO_2 in 1-ethyl-3-methylimidazolium tetrafluoroborate (EMIM BF_4) was studied in an H-type electrochemical cell, an in-situ SFG/SERS cell, and a continuous flow CO_2 electrolysis cell. Results from these experiments suggest that the EMIM BF_4 is able to catalyze the reaction in such a way that opens the door for the practical low potential and temperature conversion of CO_2.

I would like to dedicate this Thesis to my family Jordon, Sharon, and Eric

TABLE OF CONTENTS

LIST OF TABLES

LIST OF FIGURES

CHAPTER 1

INTRODUCTION

Several reports [23] issued by the U.S Department of Energy (DOE) and other governments worldwide have identified the recycling of carbon dioxide (CO_2) to useful products as one of the key challenges towards minimizing the effect of global warming and stabilizing our atmospheric CO_2 levels. Research in CO_2 conversion over the last 20 years has consistently shown low conversion efficiencies due to the large excess voltage (overpotential) required to drive CO_2 conversion. This inefficiency is the dominant reason why CO_2 capture and conversion technologies have not already been integrated into our infrastructure

Presently, there is no commercially viable process for converting carbon dioxide into fuels. According to the DOE Bell Report [23]:

"*The major obstacle preventing efficient conversion of carbon dioxide into energy-bearing products is the* ***lack of catalysts*** *… Only intermittent research has been conducted into the electrochemical reduction of carbon dioxide over the last 20 years, despite the fact that electrochemical generation of chemical products is a mature technology and already practiced on enormous scales … Electron conversion efficiencies of greater than 50 percent can be obtained, but at the expense of very high overpotentials (ca. 1.5 V).*"

Accordingly, the DOE has called for research that investigates systems that can reduce the overpotential of CO_2 conversion while maintaining high current efficiencies.

It is a highly desirable goal to convert CO_2 into fuel precursors such as carbon monoxide, ethylene, methanol, or formic acid using solar generated electricity, thereby presenting a convenient way to recycle CO_2 into fuels. In order for this goal to be achieved, we must focus on designing a system that facilitates the reduction of CO_2 to one of the above mentioned precursors at low overpotentials.

Many previous investigations have identified that the large overpotential is due to the fact that the first step in CO_2 reduction is the formation of a high energy intermediate, $(CO_2)^-$, with a standard redox potential of -1.3V vs. the standard hydrogen electrode (SHE). The purpose of this study will be to evaluate the effect of a Room Temperature Ionic Liquids (RTILs) electrolyte on the electrochemical reduction of CO_2, with particular emphasis on lowering the overpotential required to drive the reaction. Conducting the CO_2 reduction reaction in these aprotic liquids will also allow better control of the hydrogen evolution reaction, which has been shown to compete and overthrow the reduction of CO_2 as the HER reaction is thermodynamically favored.

RTILs are conceptually similar to strong acids (such as HCl) in that they are completely dissociated into ions and not diluted by any bulk solvent. They differentiate themselves from strong acids by having negligible vapor pressure at room temperature, resulting in a thermally and electrically stable liquid phase composed completely of ions.

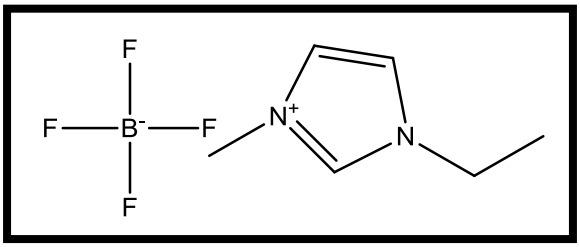

Figure 1.1: Chemical Structure of the Ionic Liquid EMIM BF_4.

In this work, we largely use the ionic liquid 1-ethyl-3-methylimidazolium tetrafluoroborate (EMIM BF_4) shown above in Figure 1.1.

We hypothesize that the ionic characteristics of some RTILs can stabilize the $(CO_2)^-$ intermediate through columbic complexation. This stabilization may dramatically lower the electrode potential required to convert CO_2. This is because the activation energy (overpotential) required to form the $EMIM^+$-$(CO_2)^-$ intermediate is lower than the energy required to form $(CO_2)^-$ without stabilization through the cation. This stabilization can have a significant impact on the energy required to convert CO_2 because it is largely agreed upon in the literature that the formation of the $(CO_2)^-$ intermediate is the rate determining step. This concept is visualized by Figure 1.2. It is for convenience of explanation that Figure 1.2 is made to resemble transition state theory, and not to suggest that transition state theory calculations would be valid in this application.

Preliminary experiments in this study have shown that in the ionic liquid 1-ethyl-3-methylimidazolium tetrafluoroborate ($EMIM^+$ BF_4^-), CO_2 reduction can begin as low as -250mV vs. SHE, and often seen even earlier under very clean and controlled conditions. Using the formal redox potential of carbon dioxide reduction in aqueous systems as a benchmark (because the formal potential in ionic liquids is not yet defined), the overpotential drops by 80% compared to a bulk of the previous literature when the conversion takes place in a RTIL. Figure 1.3 below is a representation of the carbon dioxide reduction literature over the last ten years. A vast majority of the literature reports CO_2 conversion ca. 1 volt higher than the potential derived by theory (overpotential of 1 volt). Figure 1.3 shows the calculated faradaic efficiency of our process with respect to other CO_2 reduction work over the last 10 years.

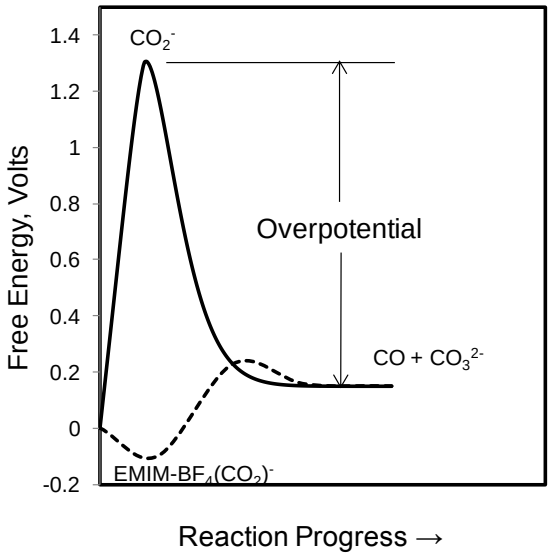

Figure 1.2: Hypothesis for How and Ionic Liquid or Amine could Lower the Overpotential for the CO_2 Reduction.

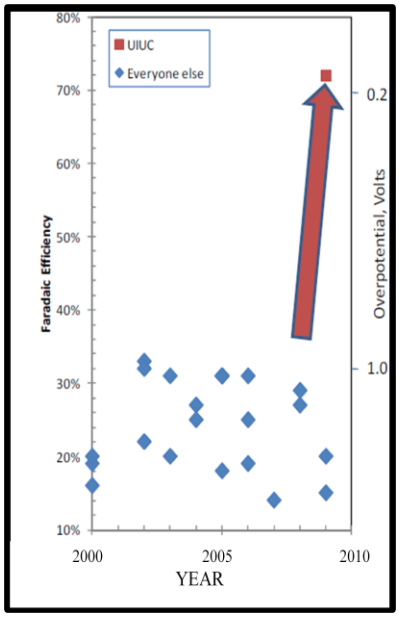

Figure 1.3: Comparison of Overpotential and Faradaic Efficiency Between this Study and Previous Works.

CHAPTER 2

BACKGROUND OF CO_2 REDUCTION AND IONIC LIQUIDS

2.1 Reduction of Carbon Dioxide

Over the past two centuries, atmospheric CO_2 concentrations have taken a rapid increase, posing many environmental threats. Carbon dioxide is among the most abundant resources on earth, and also among the most stable carbon based compounds under environmental conditions[1]. CO_2 can be converted into useful products using several techniques including (but not limited to): thermal dissociation, coupling reactions, thermal heterogeneous reactions, photochemical reduction, photoelectrochemical reduction, heterogeneous photo-assisted reduction, bioconversion, and electrochemical reduction[2]. This review will focus on the electrochemical reduction of CO_2 in both aqueous and non-aqueous environments.

2.1.1 Electrochemical Reduction of CO_2 in Aqueous Systems

Although CO_2 is not a very reactive compound, the equilibrium potential of CO_2 reduction in aqueous systems is very similar to that of the hydrogen evolution reaction (HER, Eq. 2.1) at neutral pH.

$$H^+(aq) + H^+(aq) \rightarrow H_2(g) \qquad \text{-0.414V vs. SHE @pH7} \quad (2.1)$$

$$CO_2(g) + H_2O(l) + 2e^- \rightarrow HCOO^-(aq) + OH^-(aq) \qquad \text{-0.430V vs. SHE @pH7} \quad (2.2)$$

The reduction of CO_2 in aqueous systems often must take place at large overpotentials, in part due to competition with HER. The HER can take place easily in

aqueous electrolytes by cathodic polarization, and is dominant in acidic media. On the other hand, CO_2 does not exist in basic solution; consequently, a vast majority of the literature describes CO_2 reduction taking place in neutral to slightly acidic media.

The HER is strongly dependent on the pH of the system; as the pH increases, the equilibrium potential becomes more negative. Although the reduction of carbon dioxide generates the hydroxide anion, the equilibrium potential is less dependent on pH compared to HER. As a result, under slightly acidic conditions, the HER is thermodynamically favored over the reduction of CO_2.

There are many other pathways for the reduction of carbon dioxide to various products in aqueous environments. The following is a brief list of the more prevalent reactions that have been reported along with their equilibrium potentials vs. SHE at neutral pH.

$$CO_2 + H_2O + 2e^- \leftrightarrow CO + 2OH^- \qquad \text{-0.52V} \qquad (2.3)$$

$$CO_2 + 6H_2O + 8e^- \leftrightarrow CH_4 + 8OH^- \qquad \text{-0.25V} \qquad (2.4)$$

$$2CO_2 + 8H_2O + 12e^- \leftrightarrow C_2H_4 + 12OH^- \qquad \text{-0.34V} \qquad (2.5)$$

$$2CO_2 + 9H_2O + 12e^- \leftrightarrow C_2H_5OH + 12OH^- \qquad \text{-0.33V} \qquad (2.6)$$

$$3CO_2 + 13H_2O + 18e^- \leftrightarrow C_3H_7OH + 18OH^- \qquad \text{-0.32V} \qquad (2.7)$$

It is apparent by looking at equations 2.3-2.7 that the hydroxide anion is generated as a product of CO_2 reduction in water. Consequently, the pH near the surface of the electrode is not necessarily the same as the equilibrium value. It is well known that the rate of neutralization between the hydroxide anion and CO_2 is slow in aqueous solution under ambient conditions[3]; as a result, the pH adjacent to the electrode surface is higher

than the pH of the bulk solution. CO_2 cannot exist in high pH regions, and the conversion of CO_2 is adversely impacted by the formation of this basic solution layer (similar to self inhibition schemes).

A large portion of the literature has studied CO_2 reduction in electrolytes such as $KHCO_3$ or K_2HPO_4. These electrolytes provide anions with buffing capability, and can serve to mitigate the pH effects at the electrode surface. Surface neutralization of the hydroxide anion through these buffers can take place via reactions 2.8 and 2.9 below.

$$OH^- + HCO_3^- \leftrightarrow H_2O + CO_3^{2-} \quad (2.8)$$

$$OH^- + HPO_4^{2-} \leftrightarrow H_2O + PO_4^{3-} \quad (2.9)$$

If however, the electrolyte does not have the ability to release protons, (such as KCl, $NaClO_4$, or K_2SO_4) the pH effect is enhanced as there are no ions available for neutralization.

2.1.2 Products of Aqueous CO_2 Reduction on Metal Electrodes

The products of the electrochemical reduction of CO_2 are highly dependent both on the electrolyte used, the metal surface chosen, and the cathode polarization. Many electrochemical studies have tried to focus on using metals such as Hg and Pb with high hydrogen overpotentials in an effort to suppress the HER and favor CO_2 reduction.

In a vast majority of the literature, metal electrodes that facilitate the reduction of carbon dioxide are broken down into groups based off of the major products of the reduction. Figure 2.1 below is a graphical representation of how many metal electrodes are subdivided based on the reduction products.

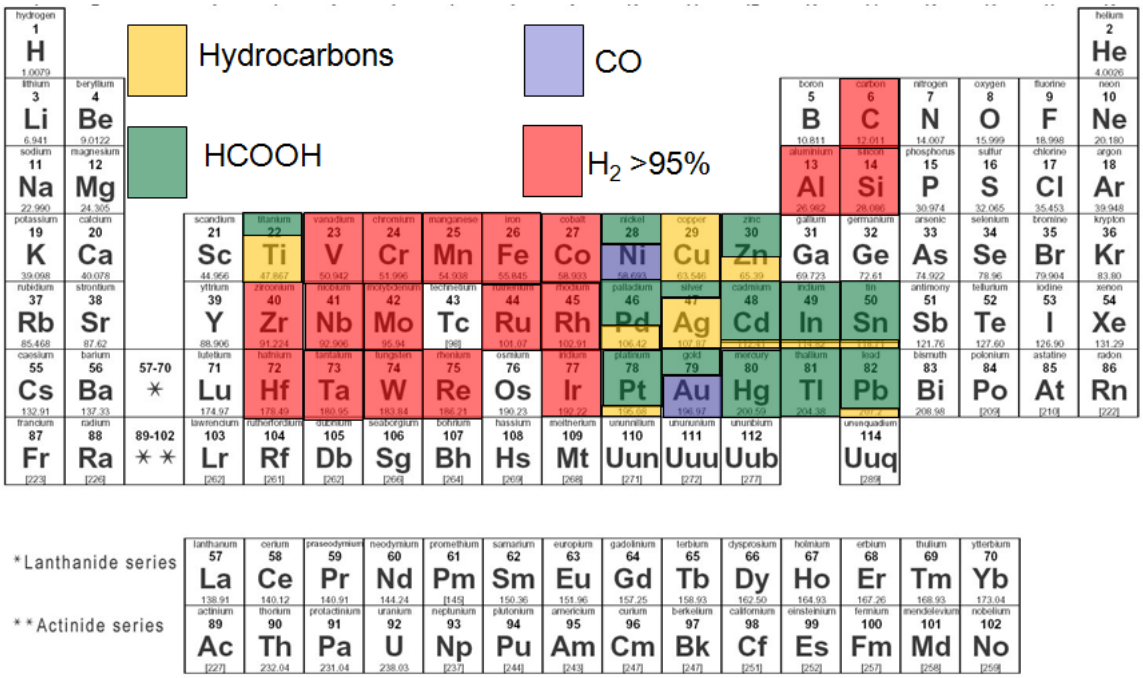

Figure 2.1: Metal Metal (Cathode) Sorted Based on CO_2 Reduction Products in $KHCO_3$ Based Media.

A majority of the 5B-7 group metals have low hydrogen overvoltage and produce most only hydrogen gas with very small amounts of CO_2 reduction product. Groups 1B, 2B and some of Group 7 metals produce various carbon based reduction products such as CO and HCOOH. More complex hydrocarbons have been reported on copper and titanium electrodes.

The information from Figure 2.1 is shown in greater detail in Table 2.1. Table 2.1 shows the general distribution of CO_2 electrolysis products as reported by different sources. It is important to note that not all metals were held at the same potential; however, a general understanding as to the overpotential required to reduce CO_2 can still be seen. The data is displayed in terms of current efficiency, which can be defined by:

$$Current\ Efficiency = \frac{current\ due\ to\ formation\ of\ product\ X}{total\ current\ measured} x\,100\% \quad (2.10)$$

Table 2.1: Reduction of Carbon Dioxide on Various Metal Electrodes in Aqueous Media.

Cathode	Potential	Current Efficientcy %				Electrolyte	Reference
metal	V vs. SHE	Hydrogen Gas	Methane	Carbon Monoxide	Formic Acid		
Cu (100)	-1.39	10.3	19.8	1.9	11.7	0.1M KHCO3	1
Cu (111)	-1.52	13.1	15.5	4.9	16.6	0.1M KHCO3	1
Cu	-1.44	20.5	33.3	1.3	9.4	0.1M KHCO3	3
In	-2.16	13.2	n.a	4.2	83.2	0.1M TEAP	2
Sn	-2.16	61.6	n.a	4.2	37.6	0.1M TEAP	2
Zn	-2.16	35.2	n.a	16.8	53.4	0.1M TEAP	2
Pb	-1.63	5.0	0.0	0.0	97.4	0.1M KHCO3	3
Au	-1.14	10.2	0.0	87.1	0.7	0.1M KHCO3	3
Ag	-1.37	12.4	0.0	81.5	0.8	0.1M KHCO3	3
Zn	-1.54	9.9	0.0	79.4	6.1	0.1M KHCO3	3
Ni	-1.48	88.9	1.8	0.0	1.2	0.1M KHCO3	3
Fe	-0.91	94.8	0.0	0.0	0.0	0.1M KHCO3	3
Pt	-1.07	95.7	0.0	0.0	0.0	0.1M KHCO3	3
Ti	-1.60	99.7	0.0	tr.	0.0	0.1M KHCO3	3
Pd	-1.20	26.2	2.9	28.3	2.8	0.1M KHCO3	3
Ga	-1.24	79.0	0.0	23.2	0.0	0.1M KHCO3	4
Cd	-1.40	39.0	0.1	14.4	39.0	0.1M KHCO3	4
Co	-1.40	102.0	0.3	0.0	0.0	0.1M KHCO3	4
Ru	-1.40	111.0	0.0	0.0	0.0	0.1M KHCO3	4
Ir	-1.40	99.0	0.1	0.0	0.0	0.1M KHCO3	4
W	-1.40	102.0	0.1	1.9	0.0	0.1M KHCO3	4
Mo	-1.40	103.0	0.0	0.0	0.0	0.1M KHCO3	4
Ta	-1.40	90.0	0.1	0.9	0.0	0.1M KHCO3	4
V	-1.40	86.0	0.1	1.1	0.0	0.1M KHCO3	4
Pb	-1.40	41.0	0.1	3.4	50.0	0.1M KHCO3	4

Metals that are generally thought of as having very high catalytic activity (e.g. platinum, titanium, ruthenium) cannot facilitate the reduction of carbon dioxide reduction in aqueous systems due to their low hydrogen overvoltage resulting in hydrogen formation at near 100% current efficiency. In aqueous systems, only metals with low hydrogen overvoltage such as Au, Ag, and Zn can produce CO_2 reduction products at high efficiency.

Despite the high current efficiency of these metals to produce carbon monoxide, it is at the expense of overpotentials nearing 1V. For example, a Zn electrode produces mostly CO at an 80% current efficiency, however the potential required to achieve this efficiency is -1.54V, which is 1V higher than thermodynamics would predict (see Equations 2.2-2.3).

An alternative theory presented in the literature is to group metals based off of the metal electronic group (i.e. sp or d) and the electrolyte type (aqueous or nonaqueous) [5]. This classification system is advantageous because it allows researchers to identify products based on the physical nature of the metal, electronic environment, and electrolyte properties[6].

2.1.3 Overpotential of CO_2 reduction in aqueous systems: Formation of $CO_2^{\cdot-}$.

Overpotential (or overvoltage) is defined as the deviation between the observed potential and the thermodynamically predicted potential required to drive an electrochemical reaction. The high overpotential associated with the reduction of CO_2 is the primary barrier preventing large scale CO_2 conversion processes from entering our infrastructure. Eliminating the sources of overpotential would therefore open the door to engineer CO_2 capture and recycle systems that would present an alternative to disposing of waste CO_2 in the atmosphere.

As previously shown, the overpotential associated with the reduction of CO_2 in aqueous environments is partly due to the competition of CO_2 reduction reactions with hydrogen evolution or water reduction reactions. However, even when metals are chosen that have high hydrogen overvoltages (thus favoring alternative reactions such as CO_2

reduction), there is still a significant overpotential that remains. This overpotential could be associated with the formation of reaction intermediates. It is largely agreed upon in the literature that the rate limiting step for the CO_2 reduction process is the formation of a high energy $CO_2^{\cdot-}$ radical anion intermediate[1, 2, 5, 6] .

$$CO_2 + e^-_{aq} \rightarrow {}^{*}CO_2^- \text{ (E°=-2.21V vs. SCE[2] in DMF)} \qquad (2.11)$$

This high energy intermediate presents a large barrier that must be overcome in order to produce reduction products and is a key obstacle towards the DOEs goal of CO_2 conversion at low overpotentials. The formation of this high energy intermediate in aqueous solvents has been reported between -1.85V [7] and -1.90V [8] vs. SHE.

Figure 2.2 below, adapted from Chaplin and Wragg[9], illustrates just how pivotal a role the $CO_2^{\cdot-}$ anion radical plays in the reduction of CO_2. In the context of Figure 2.2, this thesis will focus on the reactions A-C, namely:

Reaction "A" – Adsorption of CO_2 onto metal electrode

Reaction "B" – Single electron transfer to form $CO_2^{\cdot-}$ anion radical

Reaction "C1" – Recombination with CO_2 and electron to form CO(g)

Reaction "C2" – Recombination with proton to form adsorbed CO

Reaction "C3" – Desorption of $CO_2^{\cdot-}$ anion radical into solution

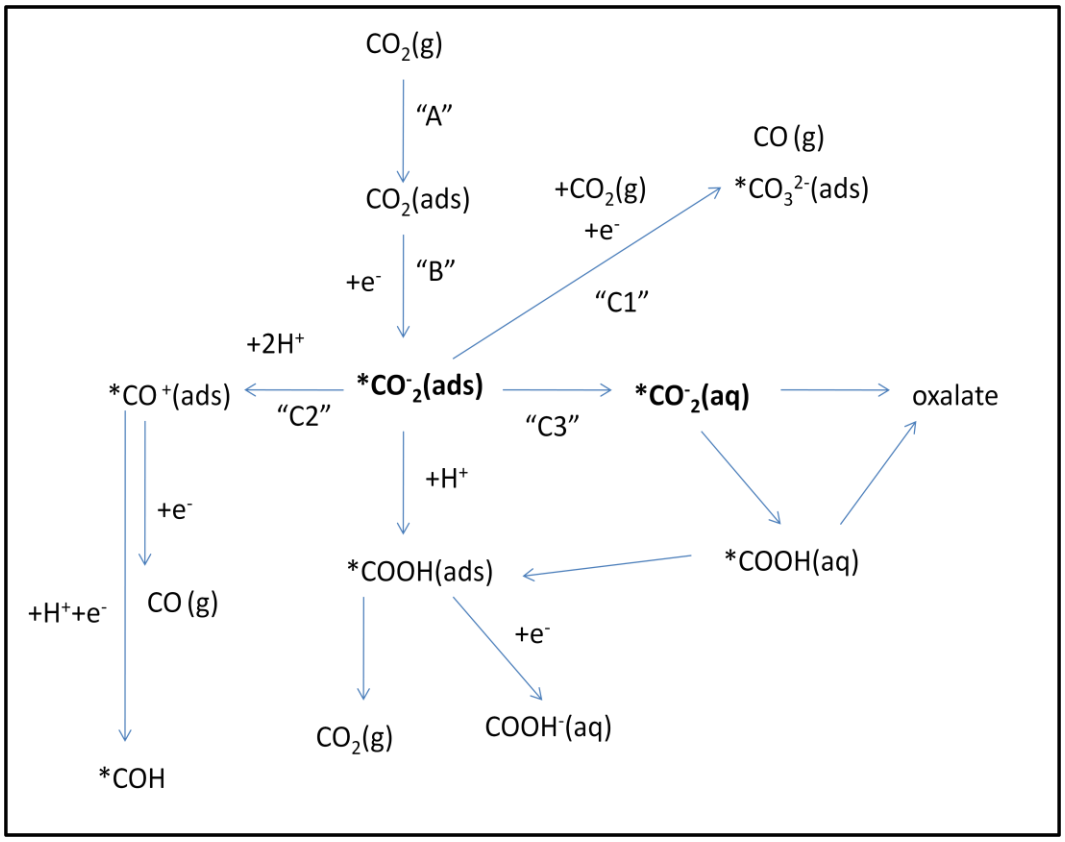

Figure 2.2: Simplified Summary of Pathways for CO_2 Reduction in Aqueous Media with Emphasis on Production of the $CO_2^{\cdot-}$ Anion Radical, CO and Formate.

2.1.4 Carbon Dioxide Reduction in Non-Aqueous Systems

Replacing conventional aqueous systems with non-aqueous systems is advantageous for three reasons: (1) The hydrogen evolution reaction can be suppressed (2) The amount of water in the system can be controlled (3) the solubility of CO_2 in non-aqueous systems tends to be higher than that in aqueous systems (ca. 33mM)[1]. Among the more popular non-aqueous solvents that have been used in previous studies include propylene carbonate (PC), acetonitrile (AcN), dimethylformamide (DMF), dimethyl sulfoxide (DMSO) and methanol (MeOH). Among this list, MeOH is an attractive solvent because it is inexpensive, produced as a (by)product on a large scale, and only slightly toxic.

In addition to the physical and engineering differences mentioned above, switching the electrolysis of CO_2 to a non-aqueous solvent has also been shown to change the product distribution using similar metal electrodes. Table 2.2 below is the methanol analog to Table 2.1 shown earlier for aqueous systems.

Table 2.2: Reduction of CO_2 at Various Metal Electrodes in Methanol.

Cathode	Potential	Current Efficientcy %				Supporting Electr.	Reference
metal	V vs. SHE	Hydrogen Gas	Methane	Carbon Monoxide	Formic Acid	in MeOH	
Cu	-2.80	5.8	68.4	15.7	6.8	500 mM LiCl	5
Cu	-2.80	3.6	6.4	35.0	17.4	50 mM KBr	5
Cu	-2.80	3.5	15.8	15.2	n.a.	50 mM KI	5
Cu	-2.80	6.2	1.0	40.0	4.8	30mM CsI	5
Pb	-2.30	5.0	0.0	2.0	75.0	300mM KOH	6
Au	-2.60	13.9	n.a	83.2	3.7	10mM LiCl/100mM TBAP	3
Pt	-2.60	17.4	n.a	66.6	7.7	10mM LiCl/100mM TBAP	3
Pd	-2.60	0.0	n.a	51.9	1.5	10mM LiCl/100mM TBAP	3
Fe	-2.60	22.2	n.a	15.6	1.4	10mM LiCl/100mM TBAP	3
Ni	-2.60	44.0	n.a	45.7	8.3	10mM LiCl/100mM TBAP	3
Zn	-2.60	0.0	n.a	89.7	n.a.	10mM LiCl/100mM TBAP	3
In	-2.60	0.0	n.a	89.2	2.3	10mM LiCl/100mM TBAP	3
Sn	-2.60	0.0	n.a	81.8	3.5	10mM LiCl/100mM TBAP	3
Cd	-2.60	0.0	n.a	61.3	1.5	10mM LiCl/100mM TBAP	3
Ag	-2.60	1.9	n.a	77.4	2.1	10mM LiCl/100mM TBAP	3

One of the first things to notice is that for all metals shown, the faradaic efficiency of hydrogen went down at the expense of larger efficiencies of other more desirable products. Additionally, many metals in methanol (supported by TBAP and LiCl) are strong candidates for use in a CO selective electrolyzer of CO_2, whereas in aqueous systems, Ag, Au, and Zn were the only reasonable contenders. In the absence of water, the mechanism for CO formation on the metal surface can be:

$$CO_2 + 2e^- \rightarrow CO + O^{2-} \tag{2.12}$$

$$2CO_2 + 2e^- \rightarrow CO + CO_3^{2-} \tag{2.13}$$

Using a categorization scheme based on product selectivity, the metals used in non-aqueous systems can be broken down into three major categories:

(1) $C_2O_4^{2-}$ producing metals: Pb, Hg, and Tl.

(2) CO production metals: Cu, Ag, Au, Sn, In, Sn, Ni and Pt.

(3) CO and $C_2O_4^{2-}$ producing metals: Fe, Cr, Mo, Pd, and Cd.

The emphasis on the production of $C_2O_4^{2-}$ is due to its potential to form several C2 (or higher) compounds depending on the proton availability of the solvent. For example the mechanism for the formation of glyoxylic acid (2.15) and glycolic acid (2.16), in non-aqueous systems with small amounts of water as described by Hori et al. is shown by:

$$2CO_2 + 2e^- \rightarrow (COO)_2^{2-} \tag{2.14}$$

$$(COO)_2^{2-} + 2H_2O + 2e^- \rightarrow HCOCOO^- + 3OH^- \tag{2.15}$$

$$HCOCOO^- + 2H_2O + 2e^- \rightarrow H_2COHCOO^- + 2OH^- \tag{2.16}$$

In addition to the importance of the solvent and metal surface, the electron mediator (supporting electrolyte) is also of critical importance for product formation and selectivity [10, 11]. For instance, Tomita et al. showed that CO_2 reduction at a Pt electrode in acetonitrile requires tetraalkyl ammonium salts such as TBAP or TEAP. A partial list of non-aqueous CO_2 reduction pathways (as cited by Hori et al.) is shown below in Equations 2.17-2.23.

$$CO_2 + e^- \leftrightarrow CO_2^{*-} \tag{2.17}$$

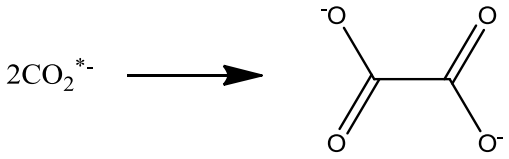

(2.18)

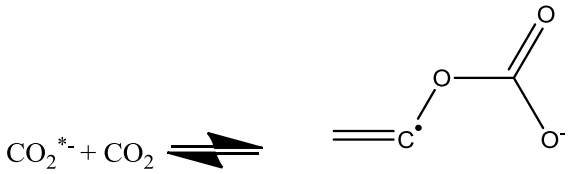

(2.19)

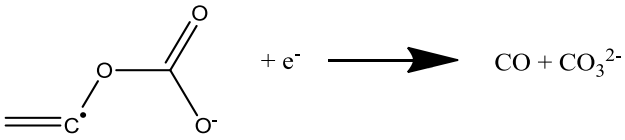

(2.20)

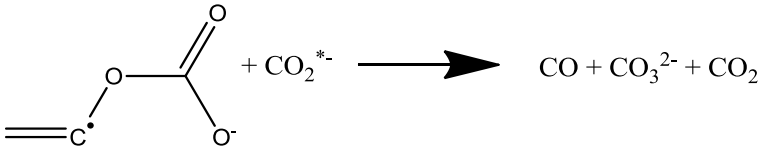

With small amounts of water:

$$CO_2^{*-} + H_2O \leftrightarrow HCO_2^* + OH^- \tag{2.21}$$

$$HCO_2^* + e^- \rightarrow HCO_2^- \quad (2.22)$$

$$HCO_2^* + CO_2^{*-} \rightarrow HCO_2^- \quad (2.23)$$

Equations 2.17-2.23, similar to Figure 2.2, shows the central importance of the initial formation of the CO_2^{*-} anion radical in non-aqueous solvents as well. In this mechanism, proposed by [10, 12, 13], a single electron transfer to adsorbed CO_2 initiates the sequence forming the anion radical. Similar to the aqueous pathways found in Figure 2.2, the non-aqueous pathways also involve the recombination of the anion radical with other radicals, CO_2, and earlier reduction products to produce more complex products.

It has also been proposed [14] that the CO_2^{*-} anion radical exists in solution and not simply and intermediate on the surface. Aylmer-Kelly et al. [15] used ultra-violet spectroscopic measurements to show the CO_2^{*-} anion radical free in solution in both aqueous and non-aqueous electrolyte solutions. It was also proposed on the basis of an observed red-shift that there is stabilization of the CO_2^{*-} via hydrogen bonding in aqueous electrolytes. In this study, another stabilization mechanism is proposed via the interaction of the CO_2^{*-} with the imidazole cation present in EMIM BF_4.

2.2 General Physical Properties of Ionic Liquids

2.2.1 Conductivity and Diffusivity

Room Temperature Ionic Liquids (RTILs) are conceptually similar to strong acids (such as HCl) in that they are fully dissociated liquids composed completely of ions and not diluted by any bulk solvent. RTILs differentiate themselves from strong acids by having negligible vapor pressure at room temperature, resulting in a thermally stable liquid phase composed completely of ions. The composition of RTILs are largely a bulky organic cation (e.g. imidazole) and an organic/inorganic anion (e.g. tratrafluoroborate, hexafluorophosphate). These ions are generally poorly coordinating, giving them the ability to be highly polar solvents without coordinating strongly to solutes. The low volatility of RTILs make these compounds more environmentally friendly compared to other organic solvents with significant vapor pressures. These liquids are also electrochemically stable having windows anywhere from 3-6 volts, making them very desirable solvents for electrochemical applications. Due to the ubiquitous nature of charge carrying ions in RTILs, there is no need for a supporting electrolyte (e.g. tetrabutylammonium phosphate) to provide sufficient solution conductivity[16].

Other physical properties of ionic liquids such as resistivity, viscosity, solubility and purity depend on the combination of ions that comprise the ionic liquid as well as the procedure used to synthesize the ionic liquid.

The conductivity of any particular ionic liquid is related to the charge density and mobility of the ions. Both of these properties are further related to the temperature and

the selected cation or anion. Table 2.3 below shows the conductivity of several ionic liquids as a function of temperature. The ionic liquids listed at the top of Table 2.3 are all $C_XMIM\ BF_4$ ionic liquids.

Table 2.3: RTIL Conductivity as a Function of Cation and Temperature; Anion is BF_4[17].

κ [S/m]	**EMIM**	**BMIM**	**HMIM**	**OMIM**
t/°C				
-25	0.106	0.008	0.002	0.001
5	0.703	0.113	0.033	0.014
25	1.546	0.352	0.123	0.058
55	3.510	1.150	0.483	0.252
75	5.230	2.000	0.926	0.512
105	8.290	3.370	1.920	1.134

Note from Table 2.3 that as the temperature increases, the conductivity of all of the ionic liquids increases as well. This is due to the decreased viscosity and hence the increase in mobility of the ions. The mobility of the ions are also dictated by alkyl chain length (for imidazole cations); note also that as the alkyl chain length increases from 2 to 8 (ethy/E to octo/O) the conductivity of the ionic liquid decreases. This decrease in conductivity with increasing alkyl chain length is also due to the decrease in mobility of the ions as the cation becomes bulkier.

Related to conductivity and mobility is the diffusion coefficient of both neutral and charged species in ionic liquids. Similar to conductivity, the diffusion coefficient is strongly dependent on the ionic liquid of interest and the charged carried by the dissolved molecule[18]. Table 2.4 below is data collected by Zigah et al. which shows the diffusion coefficient of the neutral species O_2 and the charged anion radical $O_2^{\cdot -}$ in a dilution series of (triethylbutylammonium bis(trifluoromethylsulfonyl)imide) ([Et3BuN][NTf_2]) and dimethylformamide (DMF). DMF was chosen because it can be used as a nonionic organic dilution solvent.

Table 2.4: Diffusion Coefficient of Oxygen and Oxygen Anion Radical in ([Et3BuN][NTf2])/DMF Mixture[18].

%DMF	**D (O_2)**	**D($O_2^{\cdot -}$)**	**D(O_2)/D($O_2^{\cdot -}$)**
[v/v]	[cm^2/s]		[1]
0	0.6	0.01	59
10	0.71	0.022	33
40	1.1	0.065	17
60	1.7	0.15	11
80	2.3	0.32	7.1
100	4.5	1.4	3.3

Table 2.4 shows that the diffusion coefficient is dependent both on the charge of the molecule and the composition of the liquid. Note that at all compositions, the diffusion coefficient of the oxygen anion radical is lower than that of the neutral oxygen

molecule. This is due to the interaction between the negatively charged anion and the ions in the liquid. As the ionic strength of the liquid decreases, (increasing %DMF) this interaction parameter decreases and the diffusion coefficient of the charged molecule goes up. This trend is also observed with the neutral species, however the interaction parameter between the neutral oxygen molecule and the liquid is lower compared to that of the radical. This is made clear by the decreasing diffusion coefficient ratio.

RTILs are also desirable because of their high solubility and selectivity to several gasses. For example, the solubility of CO_2 in water is approximately 30mM, whereas the solubility of CO_2 in [EMIM][BF_4] is about 2000mM (or 2M). Ionic liquids additionally show selectivity to different gasses and are often used in separation processes with hydrogen, nitrogen, and methane[19]. These separations are often facilitated by differences in solubility at either a constant temperature or at variable temperatures. For example, Finotello et al. shows that the solubility of CO_2 in [HMIM][TF_2N] decreases with increasing temperature, while the solubility of CH_4 remains relatively constant and the solubility of H_2 and N_2 increases. Table 2.5 below is data taken from Finotello that shows the Henry's Law constant (H) of several gasses in [EMIM][BF_4].

The Henry's Law coefficient is related to the concentration of dissolved gas by:

$$p = Hc \tag{2.24}$$

Where H is henrys law constant, c is concentration, and p is the partial pressure of the gas phase above the liquid.

Table 2.5: Henry's Law Constants for Several Gasses in [EMIM][BF_4].

H/[1]	CO2	N2	CH4	H2
T/°C				
25	80	7100	2900	8100
40	100	3800	2000	4140
55	130	2800	1700	2760
70	160	2300	1500	2300

It was further shown by Finotello that the solubility of various gasses in imidazolium based ionic liquids could be moderately well predicted using Regular Solution Theory (RST), which takes into account the molar volume of the solvent and solute as the primary parameter towards modeling solubility.

With all of these unique physical properties, ionic liquids are the subject of investigation for applications such as electrolytes in batteries, fuel cells, super capacitors, solar cells, electrochemical reactions, separation units, carbon capture and sequestration, and in this study, electrolyzers.

2.2.2 Structure of Ionic Liquids at the Electrified Interface

Although the structure of the ionic liquid in the double layer and at the interface is not the direct aim of this study, the behavior of ionic liquids varies significantly from conventional electrolytes at an electrified interface. There are several models that attempt to describe the organization of ions near the electrical interface; these models vary in complexity and are often only appropriate under certain conditions. Among the most well known models is the Gouy-Chapman Theory (GC). The GC model proposes that the excess charge at the electrode is neutralized by a diffuse layer of ions. This diffuse layer can be modeled by being broken down into laminae, each of a certain charge

density. The thickness of this diffuse layer depends on many factors including ionic concentration, symmetry of electrolyte and potential at the electrode surface. Using a 1:1 electrolyte, the characteristic surface thickness can be modeled using GC theory by:

$$1/\kappa = \left(\frac{\varepsilon \varepsilon_o kT}{2n^o z^2 e^2} \right)^{-1/2} \qquad (2.25)$$

Where $1/\kappa$ is a characteristic thickness, z is the ionic charge, n is the number concentration of ions in a particular lamina (0 being the bulk), T it temperature, k is the boltzman constant, ε is the dielectric constant and ε_o is the permittivity of free space. Note from equation 2.25 that as the number concentration of ions gets larger, the characteristic diffuse layer thickness gets smaller.

In the case of ionic liquids, where the number concentration of ions is very large, the diffuse layer is in fact so compact that it begins to resemble an earlier model for the electrified interface, the Helmholtz model[20]. Figure 2.3 below is a simplified schematic as to the organization of ions between the two models as well as a comparison of the potential drop profile across the layer.

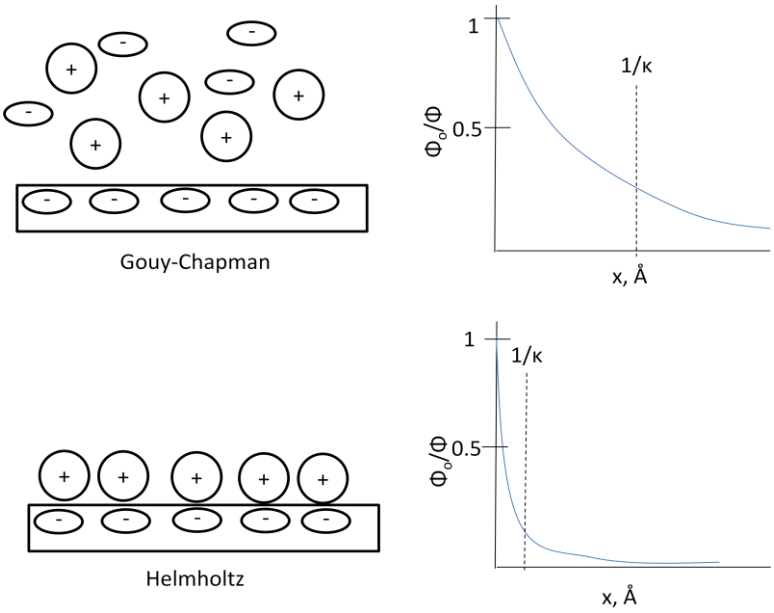

Figure 2.3: The Gouy-Chapman and Helmholtz Models for Ions at the Electrified Interface.

These two models differ both qualitatively in structure and quantitatively in the way that they describe the capacitance of the electrified interface. One need only look at the Helmholtz model of electrical organization in order to see the resemblance of the electrified interface with a conventional capacitor.

It has been proposed [21] that molten salts, such as these ionic liquids form organized layer structures at the electrified interface. This approximation "seems reasonable given the large Coulombic forces and since the layering resembles the lattice from which the liquid is derived"[20]. The capacitance for such a model is given by:

$$\frac{1}{C_D} = \frac{1}{C_K} - \frac{\delta}{\varepsilon_O\left(1 - \frac{\delta\beta\,|\,\xi\,|}{\varepsilon_O}\right)} \tag{2.26}$$

$$\delta^2 = \frac{2\varepsilon_O kT}{q^2 c_O(z-2)} \qquad \beta = \frac{\alpha q c_O(z-1)}{2\varepsilon_O kT} \tag{2.27}$$

Where ξ is the charge density on the metal, δ and β are functions of the concentration variance, z is the coordination number, q is the charge of vacancy, and α is the polarizability. Using this model, the interfacial capacitance of [EMIM][BF_4] was found to be 0.12 F/m^2. Using:

$$\frac{1}{C_D} = \frac{d}{\varepsilon\varepsilon_O} \tag{2.28}$$

The diffuse layer was found to be 5 angstroms, which is on the scale of one molecule. This result shows that even is the Gouy-Chapman model is applied, the results still lead to the limiting Helmholtz model scenario of a very tightly packed layered structure at the electrical interface where the potential drop between the surface and the bulk solution takes place over the thickness of one molecule.

2.3 CO_2 Reduction in Ionic Liquids

The reduction of CO_2 in ionic liquids is an extension of the reduction of CO_2 in non-aqueous solvents. Some of the major physical differences between ionic liquids and other non-aqueous solvents were mentioned earlier. The study of electrochemical reactions supported by ionic liquids is a new field in electrochemistry, even more so the study of CO_2 reduction in ionic liquids. Richard Compton, one of few known experts in ionic liquid chemistry, suggests two mechanisms in separate papers of interest to this study of CO_2 reduction in ionic liquids.

First, Compton reported the ability of 1-butyl-3-methylimidazolium acetate [BMIM][Ac] to reduce carbon dioxide[22]; this paper served only as a very preliminary

proof of concept as none of the products or efficiencies were reported. The main drive behind this first study was to evaluate the effect of [BMIM][Ac]'s very large solubility of CO_2 (ca. 2.5M) and attempt to maintain reducing current on a polarized platinum cathode. The large solubility, and ability to maintain current is credited to [BMIM][Ac]'s ability to complex to neutral CO_2; this claim came from the very small diffusion coefficient ($2.6*10^{-12}$ m^2/s) measured in this study. Compton concluded that the slow diffusion coefficient of CO_2 in [BMIM][Ac] was due to its strong interaction with the ionic liquid.

The second chemistry, which has helped developed the hypothesis for this study, was Compton's study of the electroreduction of molecular oxygen to its anion radical form O_2^{*-}.

$$O_2 + e^- \leftrightarrow O_2^{*-} \tag{2.29}$$

This radical is unstable in aqueous solvents as it readily reacts with water by:

$$2O_2^{*-} + H_2O \rightarrow O_2 + HOO^- + HO^- \tag{2.30}$$

and was reported to be unstable in other non-aqueous solvents. When imidazolium based ionic liquids are used, Compton proposes strong ion pairing interactions between the oxygen anion radical and the imidazolium cation, leading to a stabilized complex. It is this strong ion pairing that we wish to observe between the imidazolium cation and the CO_2^{*-} anion radical which is very crucial in the various CO_2 reduction pathways.

CHAPTER 3

EXPERIMENTAL

3.1 Materials

Electrochemistry was performed using a Solatron SI 1287 attached to a PC using CorrWare software. All of the experiments described below were conducted in a custom made glass electrochemical cell shown in Figures 3.1 and 3.2. Gasses used for electrochemistry including UHP Argon, 99.99% Carbon Dioxide, UHP Helium, Compressed Air, 99.99% Carbon Monoxide, and Nitrogen (99.99%?) were all purchased from S.J Smith Welding Supply and used as delivered. Prior to sparging any gasses into an electrochemical cell, the gasses were sent through a tube of Drierite, anhydrous calcium sulfate, in order to remove any residual moisture present in the gas streams.

The ionic liquids in this study were purchased from two different companies who manufacture ionic liquids at two different purities. The more pure, optically clear ionic liquids were purchased from EMD Chemical; these included, 1-ethyl-3-methylimidazolium tetrafluoroborate (490037.0100), 1-ethyl-3-methylimidazolium bis(trifluoromethysulfonyl)imide (490189.0100), and 1-butyl-3-methylimidazolium tetrafluoroborate (490049.0100). The less pure ionic liquid (>98%), apparent by the amber appearance, was 1-ethyl-3-methylimidazolium tetrafluoroborate (71,172-1) purchased through Aldrich.

Working electrodes were and/or supported by gold (5mm dia) or platinum (Alfa Aesar, 40419, 99.95%, 3mm dia) plugs. Platinum Black (Hi Spec 1000, Stock# 12755, Lot# H12P04, %) and Platinum Ruthenium Black (50/50 by Atomic wt.%, Stock# 41171 Lot# G24L05) were purchased from Alfa Aesar. Gold colloid (G1402-25) with a mean

particle size of 5nm was purchased through Sigma Aldrich and was stored in a freezer at -10°C. Silver nanopowder (576832-5, 99.95%) with a maximum particle size of 100nm was purchased through Aldrich. 5% Nafion (Perfluorosulfonic acid products, EW=1100) purchased through DuPont was used to bind the silver and platinum nanoparticles to the support.

The counter electrodes were made of a 25x25mm piece of platinum gauze (10283-FF, 52 mesh woven from 0.1mm dia wire, 99.9%) and purchased through Alfa Aesar. The gauze was connected to a 5" 0.5mm dia platinum wire (43288, 99.95%) purchased through Alfa Aesar.

Reference electrodes were made using acetonitrile and various ionic liquids. The reference electrode was contained by a 0.6mm OD 7.5cm long glass tube with a 1/8" long porous Vycor tip. The Vycor tip was held to the glass capillary by heat shrink. The reference electrode was made using a silver wire (99.9%) connected to a Teflon top and silver nitrate, all of which provided by BASi analytical in their non-aqueous reference electrode kit (MF-2062). Acetonitrile for the reference electrode was purchased through Fisher Scientific (A996-1 Lot#081223) with reported 0.002% water. When acetonitrile was used, the supporting electrolyte was electrochemical grade tetrabutylammonium perchlorate (86893) purchased through Fluka. The reference electrode was calibrated using Ferrocene (46260, 98%) purchased through Fluka. During the reference electrode study, a salt bridge was constructed out of Whaman filter paper and potassium chloride (P3911, 99-100.5%) purchased through Sigma Aldrich.

Cleaning reagents include sulfuric acid (98%, Batch# 13994KD) purchased through Sigma Aldrich and nitric acid (A200C212 Lot#066734) purchased through

Fischer. Nochromix© crystals (Cat# 19-010) were added to the sulfuric acid bath to create one of three cleaning solutions.

All water used in either experimentation, preparation, or cleaning, came from a DirectQ Millipore water purifier with an R-O filter (0.22 micron, SN: 0328). The water from this system measures a resistance of 18.2mΩ.

3.2 Methods

3.2.1 Preparation of the Working Electrode

The platinum and gold slugs, along with the platinum wire were cleaned of bulk oxides by suspension in 0.01M sulfuric acid at 85 °C for 3 hours. This was followed by polishing the slug with 1200 grit sandpaper (the gauze was not sanded). Residual material from the sandpaper was removed by thoroughly washing in Millipore water.

High surface area platinum and platinum ruthenium electrodes were made by preparing a catalyst ink, then depositing the ink on the surface of the polished platinum plug. The platinum (or platinum ruthenium) ink was prepared by mixing 5.6mg of platinum (HISPEC 1000, Alfa Aesar 50% Pt, 50%Ru by atomic weight) with 1ml of deoxygenated Millipore water. An aliquot of water was deoxygenated by allowing UHP argon to sparge through the water prior to use for 2 hours. The platinum/ruthenium catalyst was placed on the surface of the platinum slug by adding 5µl of the ink to the surface and allowing the water to evaporate under a heating lamp for ca. 30 min.

In several experiments, the platinum/ruthenium catalyst was supported by the 5mm dia gold slug in order to increase the total surface area of the electrode. To prepare this electrode, the same procedure is done, with the single change of adding 50µl of ink to the surface as opposed to 5µl. When the working electrode was complete, no gold surface was exposed. This was checked both before and after the experiment to ensure that no gold surface was exposed to the electrolyte solution during the experiment.

High surface area silver working electrodes were prepared by a mixing 10mg of silver nanopowder with 200µl of water, 200µl of isopropyl alcohol, and 4.6µl of 5wt%

Nafion©. The entire volume of ink was deposited onto the Platinum plug in 10µl aliquots and allowed to dry for ca. 30 min under a heating lamp and then air dry overnight.

A 0.6 mm hole was drilled laterally through the top of the gold plug and a 0.3mm hole was drilled laterally through the top of the platinum plug; these holes were used to secure platinum wire leads to the electrodes. When the gold plug was used, a 0.5mm silver wire was threaded through this hole and sent through a glass capillary creating an electrical lead; when the platinum plug was used, a 0.25mm dia silver wire was used. Note that at no point did the silver wire used to secure the working electrode to the capillary ever come in contact with the electrolyte. The capillary was then placed in a Teflon joint secured by an O-ring such that it could be secured to the electrochemical cell.

When a copper working electrode was used, a 1cm dia polycrystalline copper disc was secured by a 3mm copper wire wrapped around the outer edge of the disc. Caution was used to ensure that the wire never came in contact with the electrolyte solution. The copper wire was then connected to a silver wire and threaded through the working electrode capillary to create an electrical lead.

3.2.2 Preparation of the Auxiliary (Counter) and Reference Electrodes

The counter electrode was made by attaching a 25x50mm platinum mesh (size 52) to a 5" platinum wire (99.9%, 0.64mm dia). The platinum wire was sent through a 3mm silicone spetum followed by a nylon bushing with a 1.5mm hole and #7 threads. This assembly was threaded through a glass joint to collectively make the counter electrode.

The reference electrode was a BAS (MF 2062) silver-silver ion electrode and was prepared by adding silver nitrate at 0.01M to the either the ionic liquid under study or acetonitrile. When acetonitrile was used, it was supported by 0.1M tetrabutylammonium perchlorate. When ionic liquid was used, the silver nitrate was added to the ionic liquid after heating the liquid to ca. 80°C using a hotplate. This step was unnecessary with acetonitrile because silver nitrate is readily soluble. The reference electrode was assembled first by sealing a Vycor© frit to the tip of the glass capillary using a piece of heat shrink. The capillary was then filled with the silver nitrate solution described above and sealed at the top by a Teflon cap with a silver wire passing through.

3.2.3 The Electrochemical Cell Assembly

The electrochemical cell was made of a 25ml 3-neck flask with custom modifications. These modifications include a flattened bottom (to reduce the volume), a luggin capillary, and a sparging elbow. Figure 3.1 shows a schematic and Figure 3.2 shows a picture of the assembly. The joints that make up the working and counter electrode are secured to the neck of the flask. The third neck is simply plugged. The counter electrode is fully submerged into the electrolyte solution while the working electrode is lowered only until a meniscus is formed between the electrolyte and the lower surface of the working electrode. This ensures that only the prepared surface is under analysis.

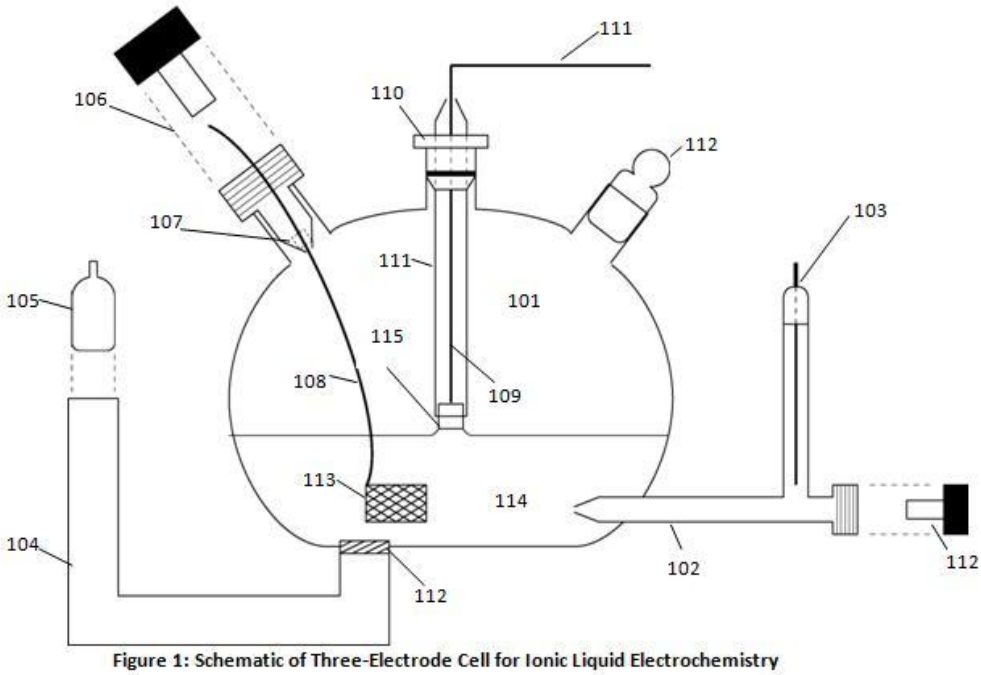

Figure 1: Schematic of Three-Electrode Cell for Ionic Liquid Electrochemistry

101- Three neck flask
102- Luggin Capillary (I.D = 1mm)
103- Silver wire and cap for reference electrode
104- Sparging tube (I.D = 4mm)
105- Lure joint for sparging gas
106- Joint for counter electrode
107- 1mm Septum
108- Platinum wire (counter)
109- Platinum wire (working)
110- Joint for working electrode with O-ring
111- Glass capillary for working electrode
112- Glass frit
113- 25x25mm Platinum gauze (size 52)
114- Ionic liquid (EMIM BF_4)
115- 0.33 cm^2 polycrystalline Pt plug

Figure 3.1: Schematic of the Electrochemical Cell.

Figure 3.2: Picture of Electrochemical Cell filled with 1-Ethyl-3-Methylimidazolium Tetrafluoroborarte (EMIM BF_4) with a Gold Working Electrode.

3.2.4 Preparation of Ionic Liquids and/or Ionic Liquid Mixtures

Prior to using any of the received ionic liquids, they were placed in a 250ml flask and heated to 105°C under a -23”Hg vacuum for at least 24 hours, a procedure cited many times in the literature [1]. Because ionic liquids are very hygroscopic (readily absorb water from the atmosphere), this procedure minimizes the amount of water and oxygen in the ionic liquid prior to use. In several experiments, water was electrochemically removed by using a glassy carbon rotating disc electrode (RDE). The electrode revolved at a fixed rate of 2000rpm in order to agitate the solution and a constant potential of -1.0V vs. Ag/0.01M Ag^+ was applied. During the RDE electrolysis of water, the counter electrode is a 25x25mm piece of platinum (52 mesh) connected to a 0.5mm platinum wire and the reference electrode was 0.01M Ag^+ in acetonitrile supported by 0.1M TBAP.

Many experiments call for either water or acetonitrile to be mixed with the ionic liquids. After the above *in vacuo* procedure, Millipore water or acetonitrile was gravimetrically added to the ionic liquid to the appropriate wt% or vol% as desired. These mixtures were kept in sealed flasks and the caps were sealed with parafilm in order to prevent the evaporation of acetonitrile and water, leading to a change in actual vol%.

3.2.5 Efficacy of Water/Oxygen Removal

After water removal steps such as *in vacuo* heating or electrolysis, the water content was accessed qualitatively by comparing cyclic voltammetry, and qualitatively through a Karl-Fischer (KF) titration. The KF titrator was an Aquatest CMA made by Photovolt. The reagent kit was Photovolt's pyridine free reagent kit (0891001). A KF titration is a coulometric titration used in analytical chemistry in order to detect trace amounts of water in dry solvents. The following is a brief description of the titration.

The anode compartment is filled with both an alcohol (ROH) and a base (B) containing both sulfur dioxide and iodine. The overall reaction (Equations 3.1 and 3.2) is the oxidation of sulfur dioxide by iodine. One mole of iodine is consumed for each mole of water present. This can be converted back to current because there are 2 moles of electrons for every mole of water present.

$$B{\cdot}I_2 + B{\cdot}SO_2 + B + H_2O \rightarrow 2BH^+I^- + BSO_3 \quad (3.1)$$

$$BSO_3 + ROH \rightarrow BH^+ROSO_3^- \quad (3.2)$$

3.2.6 Cyclic Voltammetry (CV) Monitoring Carbon Dioxide Reduction

In order to monitor the reduction of carbon dioxide dissolved in the electrolyte solution, cyclic voltammograms were taken both before and after the addition of carbon dioxide to the electrolyte solution. In order to establish a 'blank', the electrolyte was sparged (150 sccm) with UHP argon for 2 hours to remove any residual moisture and oxygen. During the blank measurement, the ionic liquid was under an argon atmosphere (ca. 1 atm). In order to electrochemically condition the surface of the working electrode, 40 CV cycles were applied at 50mV/s between -2.0V and +0.5 mV vs. Ag/0.01MAg^{+} when the working electrode was platinum, platinum ruthenium, silver or copper. When the working electrode was either gold, the positive vertex was pushed to +1.0V against the same reference because gold is less easily oxidized. Cyclic voltammetry measurements were taken at a scan rate of either 10 or 50mV/s in a stepped sweep mode with a 2Hz low pass filter and IR compensation. The reported 'blank' scan is always the last conditioning scan unless otherwise indicated. If the conditioning CV for any working electrode was not stable after 40 cycles, additional cycles were applied until the profile stabilized.

After a stable 'blank' was established, carbon dioxide was then sparged (50 sccm) into the ionic liquid for 45 minutes. The voltammetry experiments for the carbon dioxide saturated experiments followed the same specifications as the blank, except for the head atmosphere which was carbon dioxide rather than UHP argon.

3.2.7 Carbon Monoxide Stripping

The ionic liquid was first sparged with UHP argon for 2 hours as described previously. Carbon monoxide (Matheson, c.p grade) was then sparged (50 sccm) into the ionic liquid for 20 minutes while holding the working electrode at a variable potential against the 0.01M Ag^+ reference. After 20 minutes, the sparging gas was switched to argon (150 sccm) for an hour to remove carbon monoxide from solution. Carbon monoxide previously adsorbed onto the working electrode surface was held on the surface by maintaining a potential of the working electrode during the argon sparging. The potential was then scanned from the variable hold potential at 10mV/s up to +1.0V (vs. same) such that the anodic peak representing the stripping of carbon monoxide from the surface could be seen. In all subsequent scans, the peak disappears due to the lack of carbon monoxide in solution.

A variation of this experiment removes the argon purging step and holds the potential of the working electrode at a variable potential for 1, 5, 10, or 30 min. The potential is similarly scanned forward at 10mV/s from the variable potential to +1.0V such that the oxidation peaks can be seen. This procedure was carried out in pure ionic liquid, ionic liquid with 1M water, ionic liquid with carbon dioxide, ionic liquid with 1M water and carbon dioxide ionic liquid with carbon monoxide, and ionic liquid with 1M water and carbon monoxide. These experiments were all done in an attempt to differentiate the identity of the different oxidation peaks. This experiment was designed to see the effect of composition, reducing holding potential, and reducing holding time, on the nature of the oxidation products.

3.2.8 CO Coverage/Surface Area Measurements

The carbon monoxide coverage on platinum black was determined by integrating the area under the carbon monoxide stripping current-time peak (units=coulombs). Integration was carried out using Corrware software. The baseline for the carbon monoxide stripping peak was set by the profile of the second scan where the peak was no longer present due to the absence of carbon monoxide on the surface. It was previously reported [39] that carbon monoxide stripping can help determine the coverage of carbon monoxide on platinum black using the conversion constant of 420μC/cm^2.

3.2.9 Calibration of Reference Potential using Ferrocene

Ferrocene was used as an internal reference in order to calibrate our non-aqueous reference electrode. For these experiments, 2.5mM of Ferrocene was added to the electrolyte and argon gas was bubbled for several minutes in order to achieve homogeneity. It is important to note that because of the strong electrochemical activity of Ferrocene, the liquid within the luggin capillary was removed before the Ferrocene was added, then after mixing, the luggin capillary was refilled with the 2.5mM Ferrocene solution. This practice eliminates the possibility of a liquid junction potential forming across the capillary due to the presence of Ferrocene in the electrochemical cell.

3.2.10 Fourier-Transform Infrared Spectroscopy

Fourier-Transform Infrared (FTIR) Spectroscopy was used in an effort to detect species in the liquid phase dissolved in the ionic liquid. FTIR was also used to confirm

structural information about the neat ionic liquid. The data was acquired by taking a drop of ionic liquid and placing it between 2 CaF windows held together vertically by a metal frame. This setup was placed in the beam path of a Nicolet Magna-IR 760 Spectrometer. Results shown in this study are an average of 20 scans taken at a rate of about 1 scan every 2.5 seconds. The range of the scans was from 400-4000cm^{-1} with a resolution of 1cm^{-1}. In order to smooth abrupt discontinuities in the fast Fourier-transform signal, a Happ-Genzee type apodization was used.

3.2.11 Surface Enhanced Raman Spectroscopy

Surface Enhanced Raman experiments were performed using an in-situ cell described previously (Biggin, M. E. Ph.D. Thesis, University of Illinois at Urbana-Champaign, 2001.) Before each experiment the Au working electrode was electrochemically roughened in 0.2 M KCl by sweeping the potential at a speed of 75 mV/s between -0.26 and 1.24 V vs Ag/AgCl reference electrode. The working electrode was then fitted to a glass plunger with a Kel-F holder with Teflon o-ring and secured by Teflon tape. The working electrode was placed behind a quartz window (Chemglass) secured with an o-ring and screws to a Kel-F base. The 0.01MAg^{+} reference electrode was connected to the cell via a capillary bridge and a Pt wire (Aldrich) counter electrode was placed into the cell through a Teflon fitting. A He–Ne laser (λ=632.8 nm) was projected onto the sample at ~45° incidence. Scattered radiation was collected with F/4 focusing lens and focused at the entrance slit of a monochromator. A 1200 grooves/mm grating dispersed radiation onto a cooled charge-coupled device (CCD, Andor). Typical acquisition times were between 5 and 20s.

3.2.12 Sum-Frequency Generation (SFG) Spectroscopy

All spectro-electrochemical experiments in this work were conducted with the ionic liquid (IL) EMIM-BF_4 from EMD Chemical. Any residual water or dissolved gases in the IL was 'cleaned' by heating it at a temperature of ~100 ° under low vacuum conditions. Prior to the spectroscopic and electrochemical experiments the IL was purged with argon (ultra-high purity, S.J. Smith) for at least 30 minutes. Subsequently, baseline measurements were conducted to ensure a large potential window and the absence of notable amounts of water. In the succeeding carbon dioxide reduction experiments, the IL was saturated with CO_2 (99.99%, S.J. Smith) for at least 30 to 40 minutes and the spectro-electrochemical experiments were carried out.

For SFG purposes the electrochemistry were conducted in a different cell to the one used in the RDE experiments as described elsewhere [4]. The electrochemical cell for synchronized SFG and electrochemical experiments is composed of a Kel-F base with a glass cylinder attached to the top part of the Kel-F base. A glass plunger that holds the polycrystalline Au and Pt working electrodes of 6 mm diameter, is introduced through the glass cylinder and the Kel-F base. A CaF_2 optical window forms the bottom of the Kel-F base while a 50 µm Teflon spacer provides a well-defined gap between the CaF_2 window and the working electrode. This geometry allows for voltammetric scans at sweep rates of $\leq$ 5 mV/s without the detriment of strong ohmic drop effects that are associated with thin-layer electrochemistry. Cyclic voltammogram synchronized with a SFG scan were recorded with a Princeton Applied Research (PAR 263A) potentiostat using a

polycrystalline Pt wire as counter electrode and a Ag/Ag^+ (0.01 M $AgNO_3$ + 0.1 M TBAP in acetonitrile) reference electrode which was calibrated to the ferrocene redox couple as described above.

The CaF_2 optical window that is separated from the working electrode by a 50 μm Teflon spacer allows the laser beams to probe the electrode-electrolyte interface. This enables us to synchronize the acquisition of the SFG spectra of the interface with the voltammetric scans. For the SFG experiments, tunable broadband infrared (BBIR) pulses were generated in an optical parametric amplifier (Light Conversion; Topas) pumped by a femtosecond Ti:Sapphire laser system (Quantronix; Integra C series) at a repetition rate of 1 kHz. The BBIR pulses had pulse durations of ~120 fs, typical bandwidths Δ >150 cm^{-1} and pulse energies of approximately 10 and 13 μJ at frequencies Ω of 2083 and 2350 cm^{-1}, respectively. Narrowband visible pulses with 5 μJ pulse energy and a fixed wavelength of 800 nm were generated by narrowing the fs pulses to a bandwidth of <10 cm^{-1} with a Fabry-Pérot etalon. The visible pulse energy was reduced to 2.5 μJ while probing the CO vibrational bands (at an IR wavelength of 2083cm^{-1}) in order to prevent laser-induced desorption of the CO from the electrode surface. The narrow-band visible and BBIR pulses were overlapped in time and space on the electrode-electrolyte interface at an incident angle of ~60º to the normal. Sum-frequency photons were collected with a spectrograph and a charge-coupled device (CCD) with the SFG, visible, and IR photons all being p-polarized.

3.2.13 Methodology for SFG

Sum-frequency generation has been developed into a powerful vibrational spectroscopic technique for studies at surfaces and interfaces. The sum-frequency originates from a 3-wave mixing process due to the second-order polarization. The latter is induced into a material by the electric fields of a tunable infrared and a visible laser beam with a fixed frequency. The SFG intensity is proportional to the square of the interfacial nonlinear susceptibility $\chi^{(2)}(\omega_{SF} = \omega_{IR} + \omega_{vis})$ and given by:

$$I(\omega_{SF}) \propto \left|\chi^{(2)}_{NR} + \sum_q \chi^{(2)}_q\right|^2 I(\omega_{vis}) I(\omega_{IR}) \text{ with } \chi^{(2)}_q = \frac{A_q e^{i\theta_q}}{(\omega_q - \omega + i\Gamma_q)} \qquad (3.3)$$

$\chi^{(2)}_{NR}$ and $\chi^{(2)}_q$ are nonresonant and resonant parts of $\chi^{(2)}$, respectively. The resonant part is related to an orientational average $A_q \propto N\langle \mu_q \cdot \alpha_q \rangle$ of the dynamic dipole moment μ_q and to the Raman polarizability α_q of the vibration q. *N*, ω_q, Γ_q and A_q are the density of interfacial molecules, resonant frequency, damping constant and amplitude of the qth vibrational mode. It should be noted that as a consequence of Eqn. 3.3, a vibrational mode q has to be both Raman and infrared active to order be SFG active. All SFG spectra shown in the manuscript were fitted according to Eqn. 3.3 using ω_q, Γ_q and A_q as adjustable parameters.

Within the dipole approximation the nonlinear susceptibility vanishes in the bulk of centrosymmetric materials of e.g. fcc metals and liquid electrolytes. Surfaces and interfaces necessarily break the prevailing bulk inversion symmetry and give rise to non vanishing terms of $\chi^{(2)}_q$ originating solely from the interface. The interfacial

susceptibility $\chi_{IF}^{(2)}$ is still comprised of a nonresonant contribution due to nonresonant electronic excitation and a resonant contribution of dipole-allowed vibronic excitations at the interface. The SFG intensity is resonantly enhanced if the frequency ω of the tunable infrared beam matches with vibrational transitions at the interface.

3.2.14 Steady State Production of CO

The experiments described above in Section 3.2.6-3.2.13 describe the reduction of CO_2 under mass transport limited conditions. In other words, there was a limited amount of reactant available to both the cathode and the anode; furthermore, under potentiostatic conditions, diffusions gradients were allowed to form ultimately limiting the amount of reactant available to the electrode. In order to study this system under continuous conditions, a ca. 2.5cc flow cell was constructed. A cross sectional diagram of this cell is shown below in Figure 3.3.

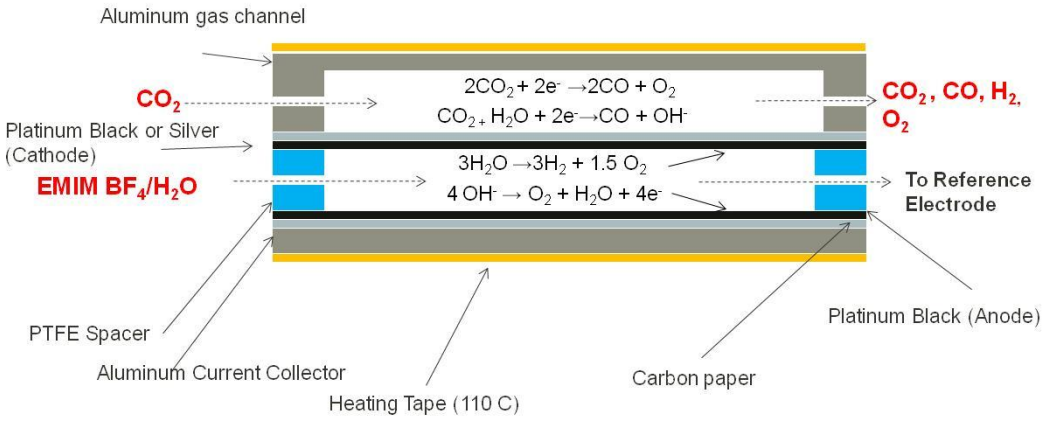

Figure 3.3: Cross Sectional Diagram of CO_2 Electrolysis Flow Cell.

Figure 3.4 shows a schematic drawing for the sections of the flow cell and Figure 3.5 is a scaled photograph of the assembled electrolyzer. From the top down, the gas channel is constructed out of aluminum. There is a 1.4mm hole drilled through either end to allow for CO_2 inlet and outlet flow. The next layer is the cathode gas diffusion layer made out of Ion Power® carbon paper.

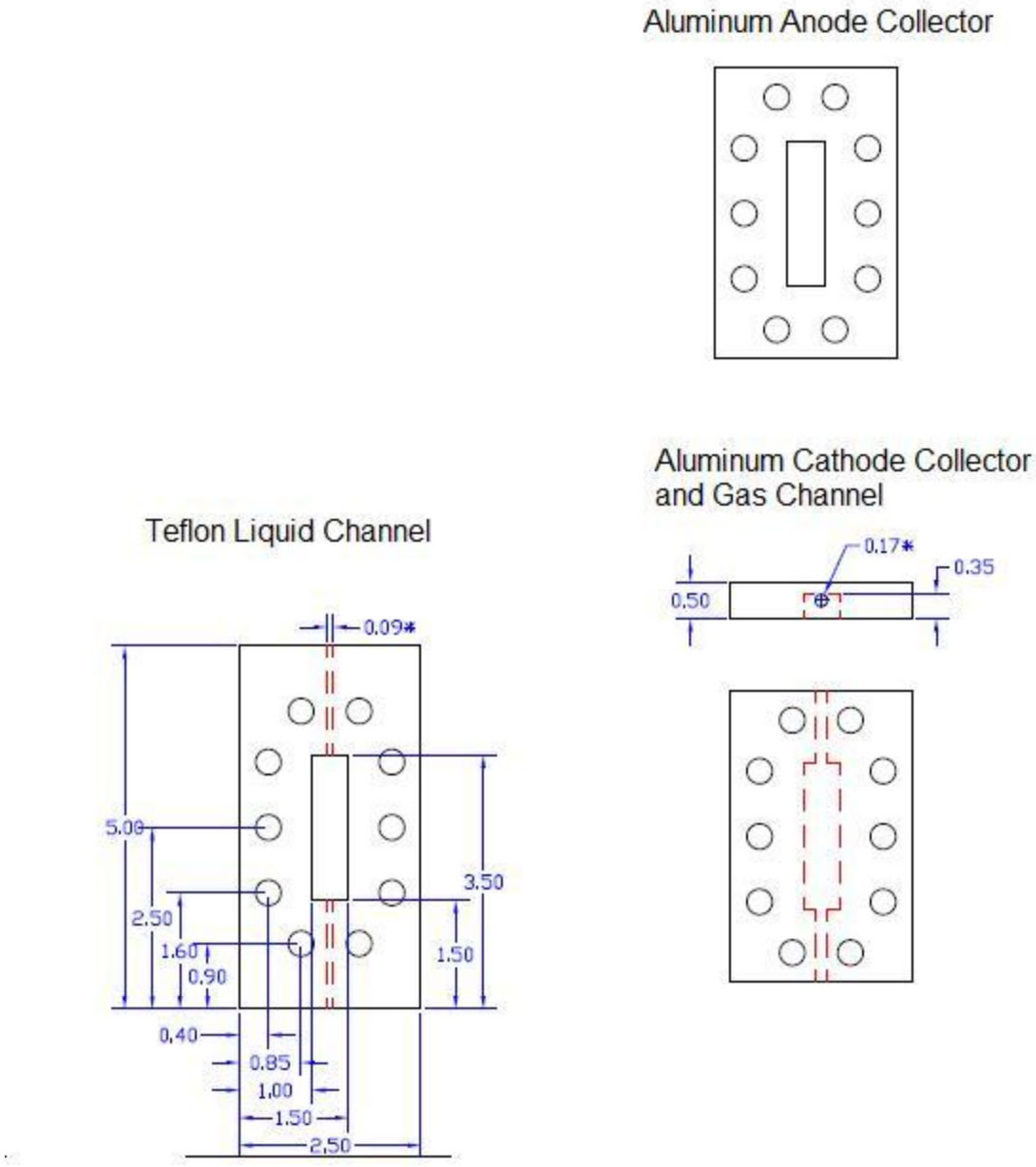

Figure 3.4: Schematic of Major Electrolysis Flow Cell Components. Figure partially made by Devin Whipple (units = mm).

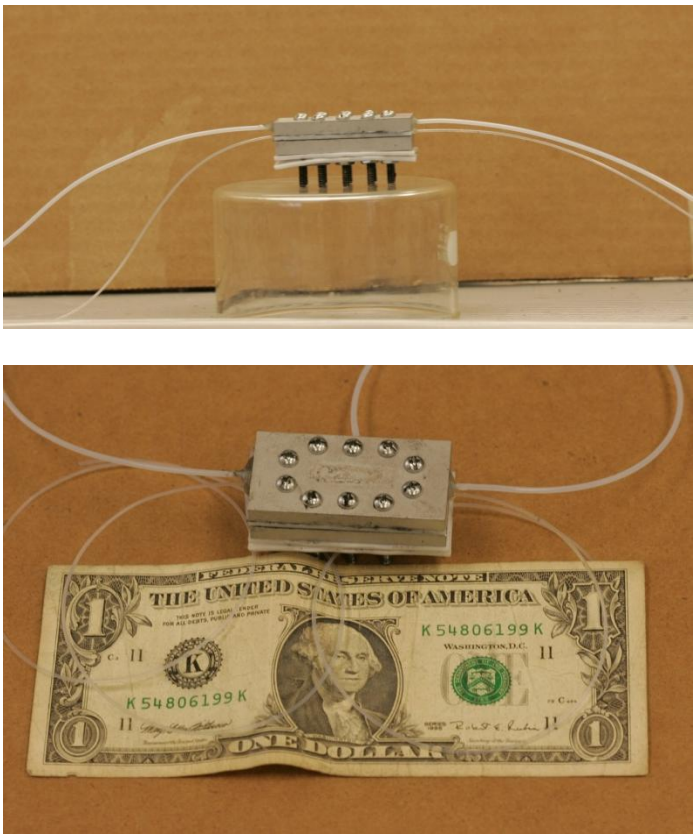

Figure 3.5. Side View of CO_2 Electrolysis Flow Cell (top) and Perspective View (bottom) of the same Cell Scaled Against a Dollar Bill.

10mg of either silver nanopowder or platinum black was painted on this 1.5cm^2 piece of carbon paper. Surrounding the carbon paper (on the same layer, not shown) is a piece of Teflon®. This serves as both an O-ring and flow block. If this layer is made completely of carbon paper, CO_2 would have the ability to diffuse out the sides of the reactor. The next layer is a Teflon liquid channel with 0.9mm holes drilled on either end to allow for liquid inlet and outlet flow. Below the liquid channel is the gas diffusion layer for the anode. In all cases, 4mg of Pt black was painted on a 1.5cm2 area in the middle of the gas diffusion layer. Because no flowing gas is in contact with this layer, the entire layer is made out of carbon paper as lateral diffusion is not a large concern on the anode. Beneath

the anode is another aluminum plate, which serves both as a support for tightening the reactor, and as a current collector (note the cathode current collector is the gas channel itself). Because metallic (zinc) bolts are used to hold the reactor together, it is necessary to both wrap the top portion of the bolt with Teflon tubing and include 2 layers of Teflon below the anode current collector in order to prevent short circuits by way of the bolts. Prior to starting any experiment, the resistance of the cell was measured with a multimeter. A resistance on the order of megaohms was deemed as an acceptable resistance to begin testing. A resistance lower than this value generally suggested that the carbon paper, bolt, or liquid residue was providing a connection between the electrodes and shorting the cell. The inlet gas channel was connected via a hypodermic needle to a CO_2 MFC (Dakota). In all experiments, the flow rate of CO_2 provided to the flow channel was 2.5 sccm. The liquid channel inlet was attached to a syringe pump filled with the appropriate liquid phase. In aqueous experiments (including 82% vol water + EMIM) , the flow rate was 500µl/min. In ionic liquid phase experiments, the flow rate was approximately 1ml/min; this difference is to compensate for the large pressure drop in the channel due to the high viscosity of the ionic liquid.

The gas phase outlet was attached to a SRI Gas Chromatograph with Peak Simple v3 software. The column oven was kept at 100C, and the TCD detector was kept at 110C. The column used was a 6’ molecular Sieve (type 5A) column. Advantages to this column choice include the ability to separate carbon monoxide from hydrogen, nitrogen, and oxygen; however, it is noted that this column performs poorly under CO_2 carrier conditions as generally CO_2 is unable to make it through the column. Due to the small

injection size (100µl), the column is able to support many injections before the CO_2 "poisons" the columns ability to effectively separate the gas effluent.

The liquid channel outlet was connected to a scintillation vial where liquid effluent was allowed to accumulate in contact with the Ag/Ag^+ reference electrode. The capillary leading from the channel to the vial acted as a salt bridge. It is presumed that because of the small diameter and length of this bridge, the solution resistance is negligible as this bridge acts as a luggin capillary.

Electrically, the cathode and anode were attached to the Solatron and biased only with respect to each other (i.e. cathode = -2, -2.25, -2.5, -3 vs. anode). In order to measure the polarizations of the electrodes, both the cathode and anode were attached to the reference electrode using multimeters.

CHAPTER 4

ELECTROCHEMICAL RESULTS AND DISCUSSION

4.1 CO_2 Reduction in EMIM BF_4

4.1.1 Linear Sweep Voltammetry

Previous reports [1] have discussed the advantages of performing CO_2 reduction in non-aqueous solvents such as acetonitrile and methanol. Advantages to these solvents include the mitigation of hydrogen evolution, a significant source of overpotential in aqueous systems. Accordingly, the literature has shown [5] that CO_2 reduction can begin at slightly less negative potentials in these systems compared to the reduction taking place in water. Like aqueous systems, electrochemistry performed in acetonitrile and methanol requires a supporting electrolyte, generally 100mM tetrabutylammonium perchlorate (TBAP) or sulfuric acid. The following study represents the electrochemistry of CO_2 reduction in the ionic liquid 1-ethyl-3-methylimidazolium tetrafluoroborate (EMIM BF_4). EMIM BF_4, as described previously, is completely ionic, obviating the need to introduce a supporting electrolyte into the solution to maintain sufficient conductivity. The ionic liquid was purified using the techniques described in Section 3.2.4 and placed into the working compartment of an H-type electrochemical cell. The working electrode was HiSpec platinum black supported on a 0.5mm dia. gold plug. The catalyst ink was made by sonicating 5.6mg of platinum black in 1ml of water, and subsequently depositing 50µl of this ink onto the gold plug. The droplet, supported by the

plug, was then placed under a UV heating lamp for 30 minutes and allowed to air dry for at least an additional 30 minutes. The counter electrode was a 25x25mm piece of platinum gauze,52 mesh, woven from 0.1mm dia wire, connected to a 5" 0.5mm dia platinum wire. The wire pierced through a nylon septum and Teflon bushing to maintain airlock. The reference electrode, separated from the working compartment by a 1mm I.D. luggin capillary, was a Ag/Ag^+ electrode made by adding 0.01M silver nitrate and 0.1M TBAP to acetonitrile and inserting a silver wire. It was determined that there is a +631 shift between this reference system in contact with EMIM BF_4 and the SHE electrode. In all the following data, the potential scale will be against the SHE system. It is important to note that we used ferrocene as the standard in order to calibrate the magnitude of the shift. This procedure is widely cited in the literate as the ferrocene couple is a stable, reproducible, one electron redox couple.

The keystone data plot shows how electrons begin to flow into solution to facilitate the reduction of CO_2 and formation of CO_2^- at ca. -0.2V, which is 400mV earlier compared to the already advantageous system of acetonitrile. Figure 4.1 below shows a direct comparison of the acetonitrile system compared to the EMIM BF_4 system. The point at which electrons begin to flow into solution is taken as the point at which the CO_2 saturated solution produces a more negative current compared to the argon saturated solution. This is confirmed by SFG experiment described later in this work.

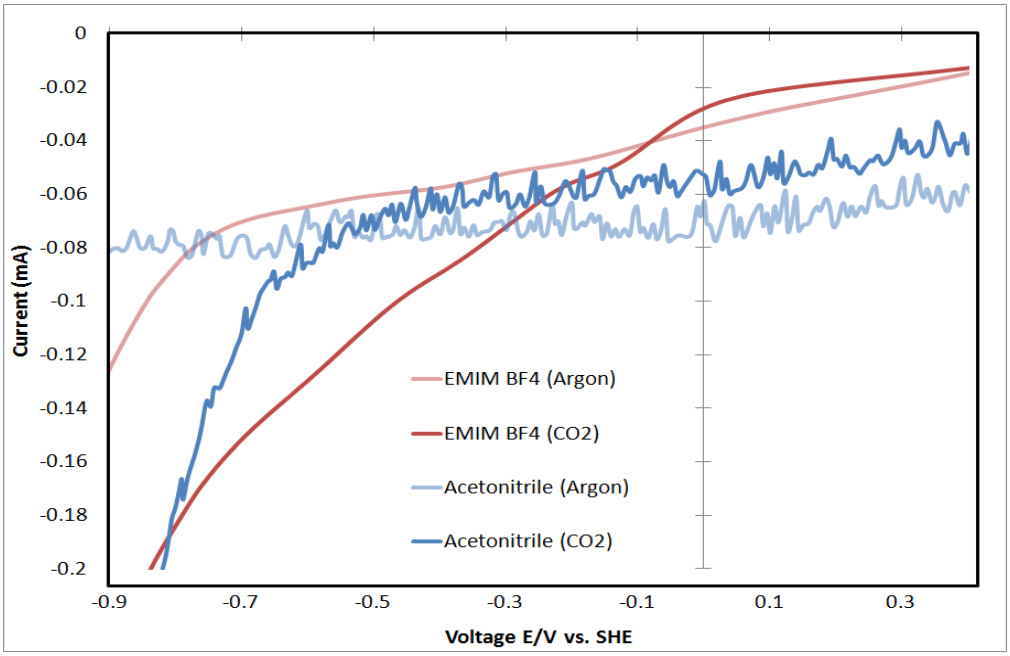

Figure 4.1: Reduction of CO_2 in EMIM BF4 Compared to Acetonitrile.

The reduction in overpotential for CO_2 in EMIM BF_4 compared to acetonitrile (and water) is rooted in the stabilization of the CO_2^- anion radical on the surface by the $EMIM^+$ cation. The stabilizing complex, denoted as CO_2^--$EMIM^+$ forms a potentials just under 0.1V and is readily stabilized by the ubiquitous $EMIM^+$ cations. This compares to potentials near -1.7V required to form the CO_2^- anion intermediate in aqueous systems. As will be discussed later, only the presence of an electrified interface in conjunction with a liquid co-catalyst (EMIM BF_4) will facilitate the early formation of $EMIM^+$-CO_2^-. This result was confirmed by the absence of any Raman-active CO_2 bands in CO_2 saturated EMIM BF_4, and the presence of those asymmetric transitions with an electrified surface (using SFG).

Next, the ability of EMIM BF_4 to co-catalyze CO_2 reduction was assessed using catalyst blends. Figure 4.2 below shows a comparison of CO_2 reduction in EMIM BF_4 on Pt black compared to the same area of Pt-Ru black. The inset of Figure 4.2 shows that CO_2 reduction begins ca. 140mV more negative using Pt compared to Pt-Ru in EMIM BF_4. Despite this difference, the Pt-Ru catalyst outperforms the Pt catalyst at larger overpotentials.

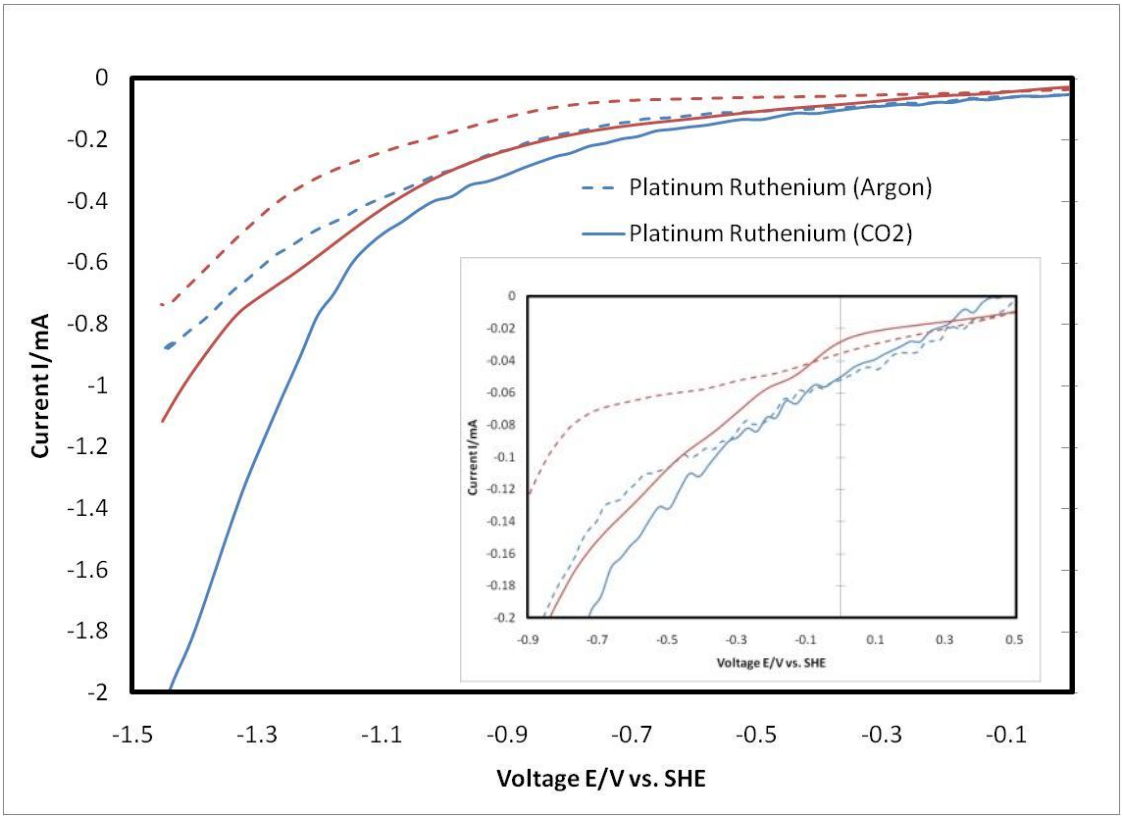

Figure 4.2: Reduction of CO_2 on Pt black and Pt-Ru black in EMIM BF_4; Inset at Low Overpotential.

This means that the bi-functionality of the catalyst is more helpful in maintaining and facilitating the production of products at moderate overpotentials, but less efficient at the initial electron transfer to CO_2 at the interface This suggests that the platinum atoms

are predominantly responsible for catalyzing the initial electron transfer and that ruthenium is able to catalyze the latter electrochemical steps.

Finally, we wished to assess the ability of EMIM BF_4 to co-catalyze CO_2 reduction on a non-platinum metal known to have a high Faradaic efficiency of CO_2 conversion in aqueous systems. From Table 2.1, we see that gold is among a small group of polycrystalline metals known to be very active in CO_2 reduction in aqueous systems. Figure 4.3 below is a cyclic voltammogram (ν = 50mV/s) of CO_2 reduction in EMIM BF_4. Note how the reduction is characteristically different in this scan compared to the scans shown in Figures 4.1 and 4.2 above. Although the reduction of CO_2 is still occurring, the initial electron transfer occurs near -500mV, a much more negative value compared to the data on Pt and Pt/Ru above. Additionally, a full Faradaic wave (ca. 1.1V) is seen in the reduction of gold; this is most likely due to the significantly smaller surface area of our gold cathode compared to the high surface area Pt and Pt/Ru cathodes. In the case of Au, we reach a mass transfer limitation and see the faradaic wave.

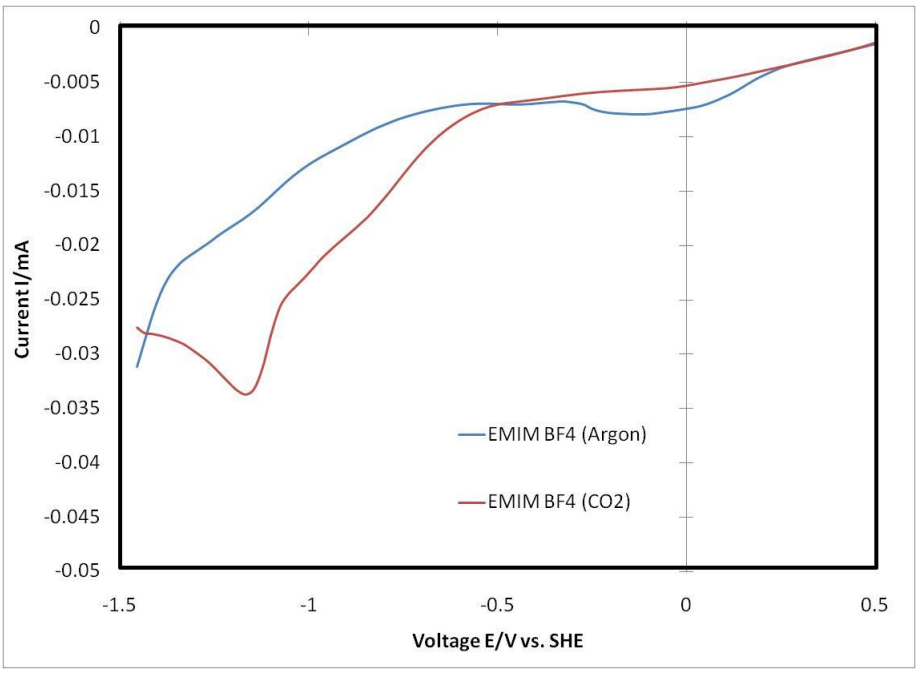

Figure 4.3: CV of CO_2 Reduction on an Au Plug (5mm dia) in EMIM BF_4.

It is then perhaps a morphological effect that led to the result using the Au electrode where CO_2 gets reduced at more negative potentials. As seen in Figure 4.3, the current is much lower using the polished gold electrode compared to the high-surface-area Pt inks (as would be expected). While the Platinum/blended catalyst was high surface area nanoparticles, the gold electrode was a highly polished plug. In order to ensure the differing results between the platinum/blend catalysts and the gold catalyst was not a morphological effect, the reduction of CO_2 on gold was repeated using an electrochemically roughened gold electrode. The procedures for electrochemically roughening the gold plug involve placing the gold plug in 0.2 M KCl and sweeping the potential at a speed of 75 mV/s between -0.26 and 1.24 V vs. Ag/AgCl reference

electrode. This is the same roughening process used in Surface Enhance Raman Spectroscopy (SERS) experiments, creating a gold electrode with nano-size roughness properties, comparable to the deposition of depositing nanoparticles on a metal support. Figure 4.4 below shows CO_2 reduction in EMIM BF_4 on the roughened gold electrode.

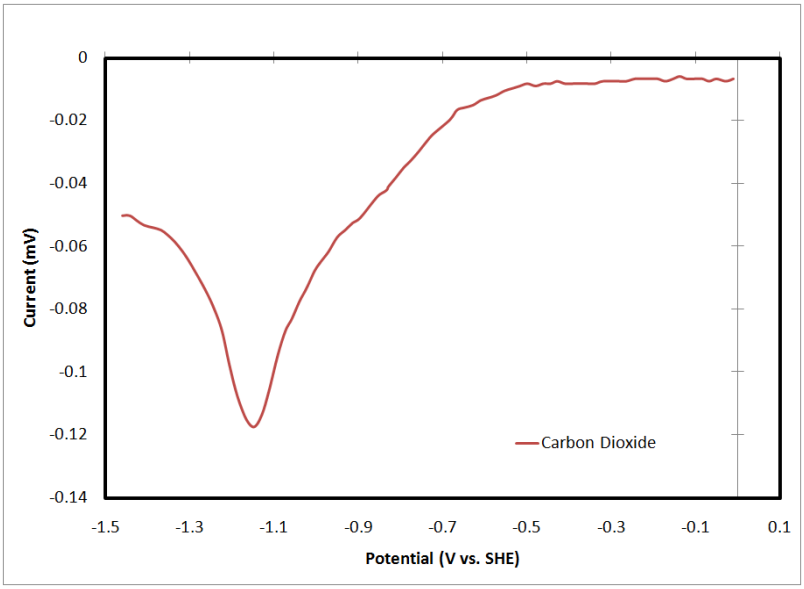

Figure 4.4: Reduction of CO_2 on a Roughened Gold Electrode in EMIM BF_4.

Note from Figure 4.4 above that even under the roughened morphological conditions, the reduction of CO_2 still begins at -500mV, and there is still a full cathodic wave just under -1.1V representing a different redox chemistry compared to the platinum/blend catalysts.

4.1.2 Cyclic Voltammetry of CO_2 reduction in EMIM BF_4

When trying to study novel electrochemical systems, cyclic voltammetry is an excellent diagnostic technique used to attain a broad knowledge about the electrochemical activity of the system. Separate from linear sweep voltammetry, cyclic voltammetry sweeps the potential between two vertices for a pre-determined number of cycles. Prior to the true experiment, it is often it is necessary to remove bulk oxides and impurities from the catalyst surface by continuously cycling the working electrode between two potentials below the oxidation potential of the metal. All voltamogramms shown are the final cycle, representative of the repeatable and steady electron transfer topology of the system. Figure 4.5 below is a cyclic voltammogram of argon saturated EMIM BF_4 (blue) and CO_2 saturated EMIM BF_4 on a Pt black surface.

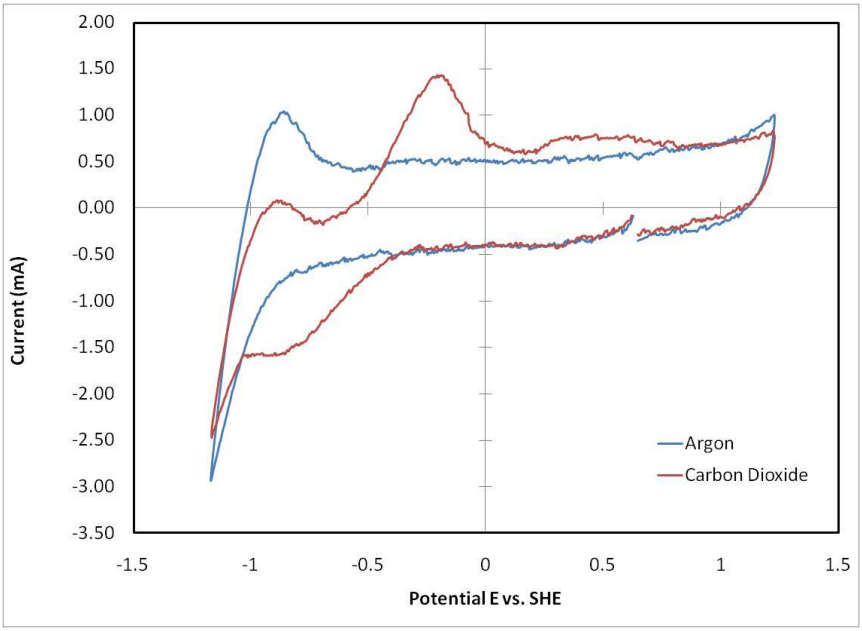

Figure 4.5: CV of Argon and CO_2 in EMIM BF_4.

In order to make the reduction and oxidation peaks less ambiguous, they can be paired by varying the more negative vertex in an effort to link novel reduction and oxidation peaks.

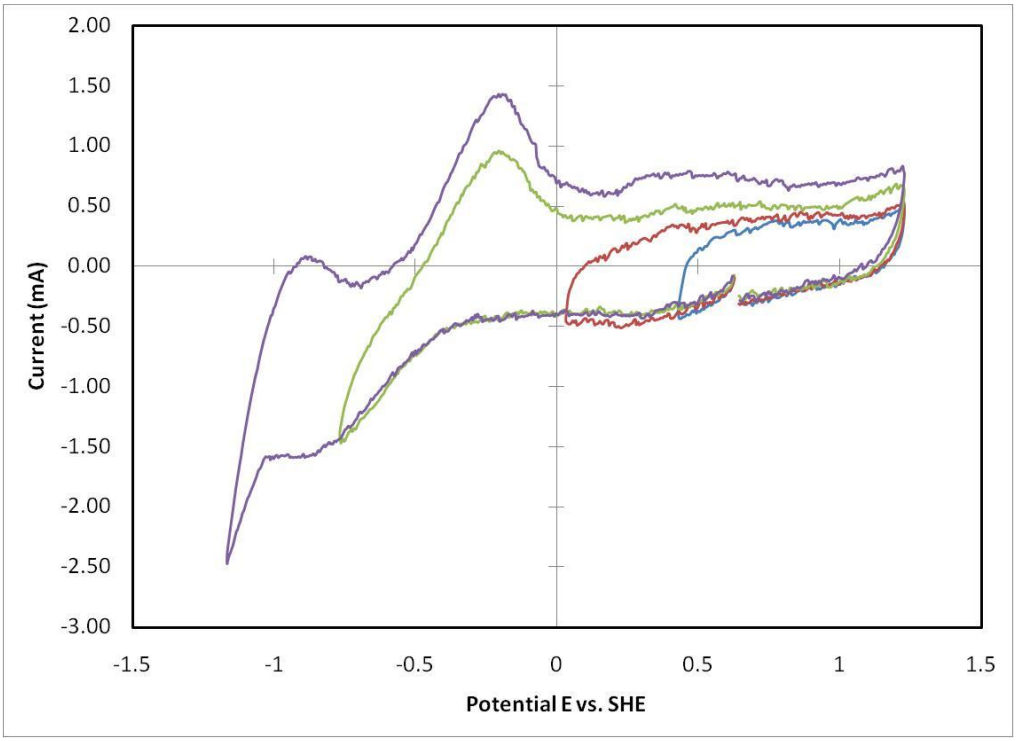

Figure 4.6: Variable-Vertex CV of CO_2 in EMIM BF_4.

From Figure 4.6 above, it can be seen that there is one novel reduction wave beginning at ca. -300mV and two novel oxidation waves peaking at ca. -300mV and +500mV. The reduction occurring at ca. -1.1V and subsequent oxidation at -1.0V is a background wave due to the solvent. This figure suggests that CO_2 is reduced on platinum, but then oxidizes either to two different species or to the same species via two different routes(as suggested by the two oxidation peaks).

Karl Fischer titration studies have shown that EMIM BF_4, prior to being charged into the cell, has approximately 80mM of water in it. As a result, CO_2 can be reduced via two different pathways.

$$2\ CO_2 + 2e^- \rightarrow 2\ CO + O_2^{2-} \quad (4.1)$$

$$CO_2 + H_2O\ 2e^- \rightarrow CO + 2OH \quad (4.2)$$

Equations 4.1 and 4.2 above represent the dominant non-aqueous and aqueous pathways for CO_2 reduction respectively, which given the reaction conditions and oxidation waves, are both occurring on the surface. The oxidation wave occurring at -500mV is most likely the reverse of the initial electron transfer to CO_2. The more positive peak occurring at +500mV is most likely the aqueous oxidation route from CO to CO_2. This value is in agreement with the literature for CO oxidation of Pt in aqueous systems.

4.1.3 CO_2 reduction in EMIM BF_4-H_2O Mixtures

As described by this work, the CO_2 reduction reaction and the water reduction reaction are not independent entities. As shown by Figure 4.7, a controlled amount of hydrogen on the surface of the cathode can promote alternative routes for conversion and subsequent oxidation off of the surface. Additionally, CO_2 reduction in the presence of water produces hydroxides at the surface of the cathode (thus changing the pH) which changes the kinetics of both CO_2 reduction and water reduction at the electrode. Furthermore, during CO_2 reduction, the surface is covered in CO (whether or not CO be the final desired product or not). For platinum, CO acts as a poison which inhibits further CO_2 conversion as the surface sites disappear; if however a small (i.e. 10-500mM)

controlled amount of water is in solution, the surface turnover rate can increase leading to higher conversion rates. This principle is shown below in Figure 4.7.

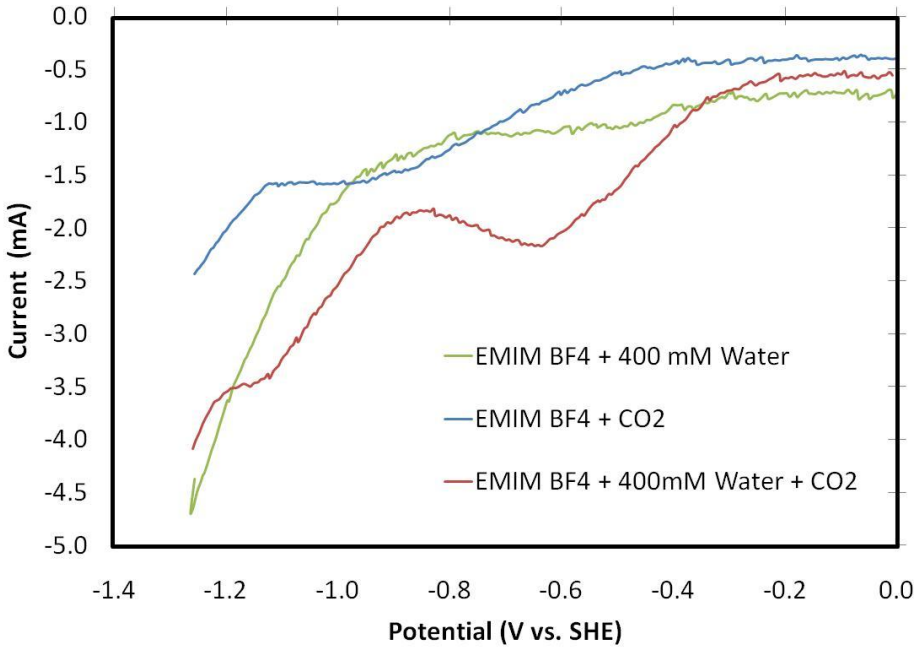

Figure 4.7: CO_2 Reduction in EMIM BF_4 and EMIM BF_4-H_2O Mixtures.

The reduction of CO_2 in pure EMIM BF_4 shown above is very similar to the previously shown data. When 400mM of water is added to the working electrode compartment, we see an increased current in the region of CO_2 reduction (-200mV to -800mV), to the point where there is a mass transfer limitation and the full faradaic peak for the conversion of CO_2 is observed. As described earlier, an increase in current for CO_2 reduction in the presence of water is not necessarily due to the increased conversion of CO_2. In order to help discriminate between the competing reactions, the same experiment was run using only EMIM BF_4 and 400mM water. Note that no faradaic peak is observed in the CO_2 conversion region in the EMIM BF4-H_2O system, and that the

cathodic shoulder that begins to form at about -0.9V in this system is identical to the shoulder that forms in the EMIM BF_4-H_2O-CO_2 system. This data suggests that the current due to the conversion of water is largely seen in the -0.9V region, and that the additional current observed in the CO_2 conversion region is largely due to the increased rate of CO_2 reduction. This is a very interesting result, because it shows that we have lowered the overpotential for the desired CO_2 reaction while at the same time we raised the overpotential for the water reduction reaction by about 100mV to -0.9V.

$$H_2O + 2e^- \rightarrow H_2 + 2OH^- \qquad \text{(E° -0.8V vs. SHE)} \qquad (4.3)$$

In the context of the broader goals of this project, this experiment represents the concept that this system can be optimized with respect to the role water plays in the reduction on CO_2. On the one hand, too little a water concentration will lead to a low turnover rate on platinum as the adsorbed CO will have limited pathways of oxidation off of the surface which would require this process would then use large anodic overpotentials. On the other hand, as described in the introduction, too much water will lead to a surface covered in hydrogen leaving no room for CO_2 conversion unless a large overpotential (1.0-1.5V of overpotential) is applied. Under these experimental conditions, this experiment shows the amine-regulated suppression of hydrogen evolution and the amine-regulated stabilization of CO_2 conversion. In other words, this system shows it is possible to raise the overpotential of undesired reactions (HER) while simultaneously lowering the overpotential of desired reactions (CO_2 conversion).

4.1.4 Cyclic Voltammetry of CO_2 Reduction in EMIM BF_4-Water Mixtures

In an experiment similar to the one described in Figure 4.5 and Figure 4.6, the variable vertex technique was utilized in order to probe the EMIM BF_4-H_2O system. Below in Figure 4.8, the cyclic voltammogram (υ=50mV/s) of this system is shown. When comparing Figure 4.8 with the analogous "dry" version of this experiment (Figure 4.5 above), we see that there is an extra set of redox peaks in the presence of water. The additional reduction wave is found to reach a mass transport limitation around -1.0V vs. SHE, and its correlated oxidation wave is found to peak at ca. -800mV vs. same. To validate the relationship between the three redox couples (CO_2, water, solvent redox chemistries), Figure 4.9 shows the result of the variable vertex experiment.

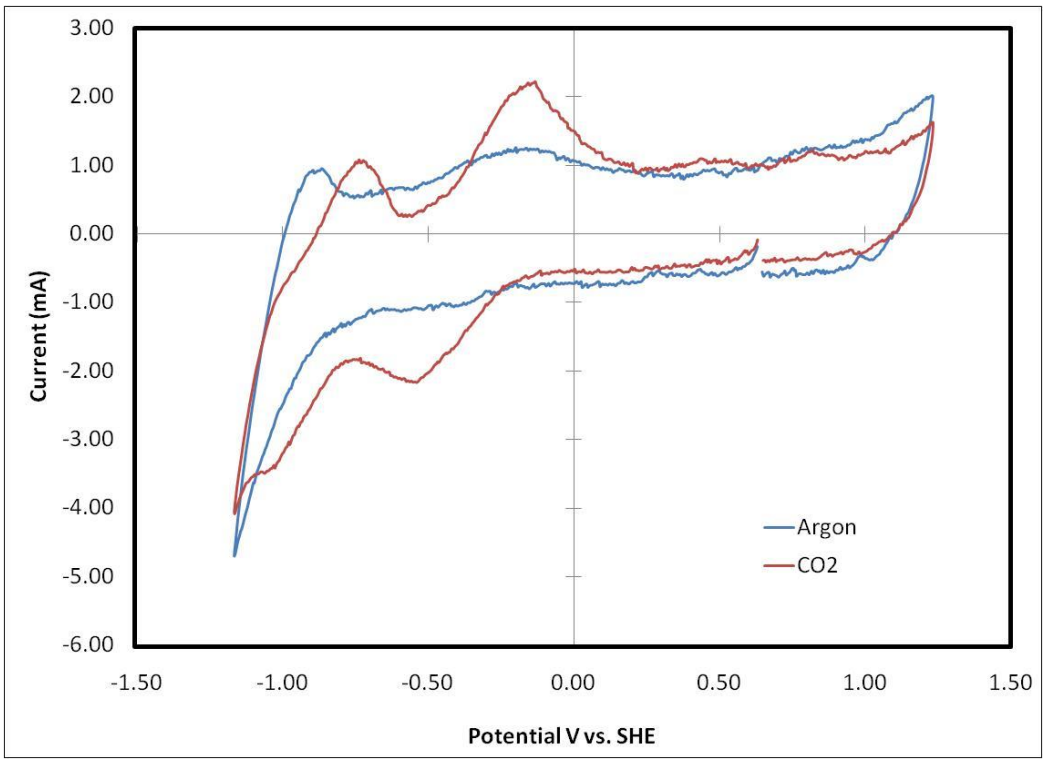

Figure 4.8: CV of EMIM BF_4-H_2O (400mM) System.

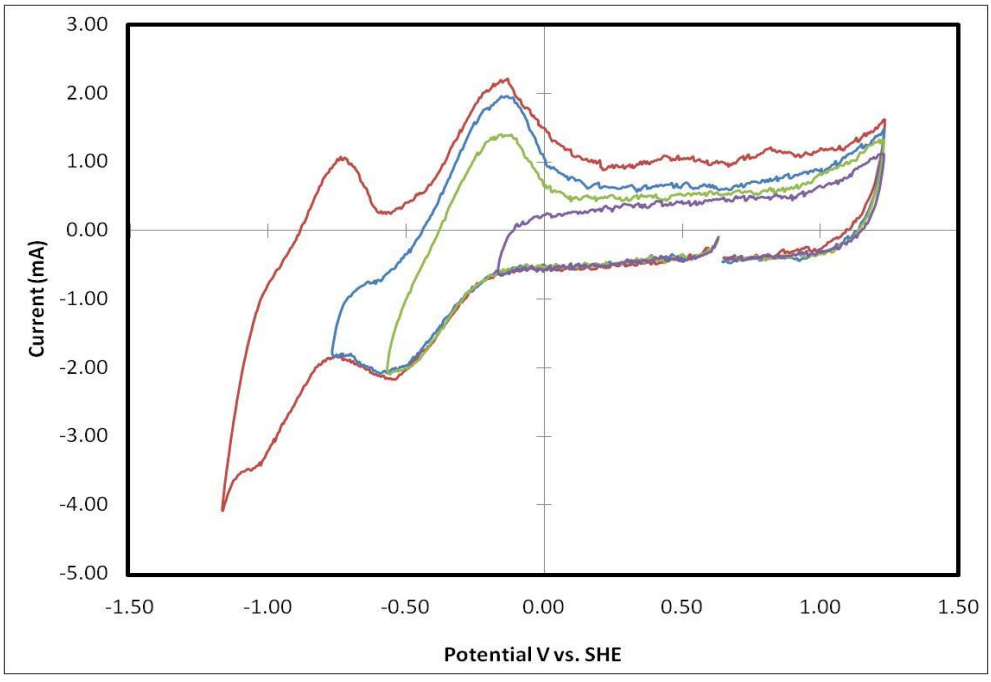

Figure 4.9: CV of EMIM BF_4-H_2O-CO_2 System.

4.1.5 CO_2 Reduction in 18mol% EMIM BF_4 in Water

Analogous to the dry EMIM BF_4 system, we also wished to assess the performance of catalysts that are known to have good CO_2 conversion efficiencies in aqueous systems. Because gold and silver are known to be good catalysts selective to CO formation in aqueous systems, a significantly larger amount of water may be added to the system without fear of large CO_2 conversion overpotentials. It is also important to note that no supporting electrolyte was added to the water phase of this mixture as the ionic liquid provides the mixture with sufficient conductivity to perform the electrochemistry. Berrose [22] et al. shows that there is a peak in the conductivity in EMIM BF_4-H_2O mixtures at 18mol% EMIM BF_4, which is the concentration used in the following Figures 4.10, 4.11, and 4.12. For clarity, note that Figures 4.10, 4.11, and 4.12 are not plotted on a common scale, either on abscissa or ordinate.

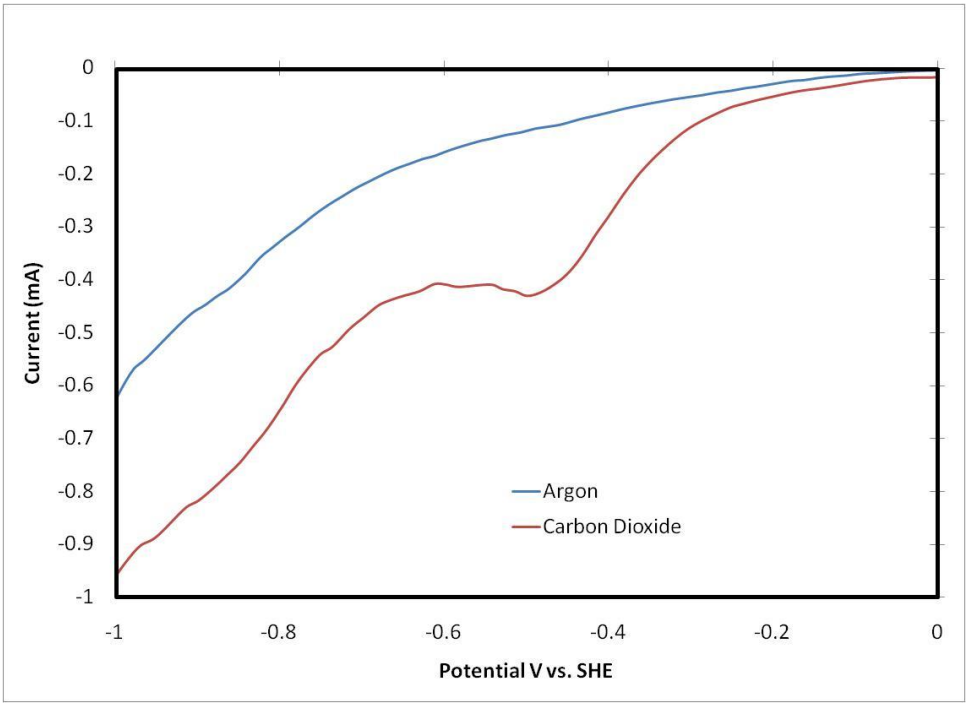

Figure 4.10: CV of CO_2 Reduction on Roughened Gold in 18mol% EMIM BF_4 in Water.

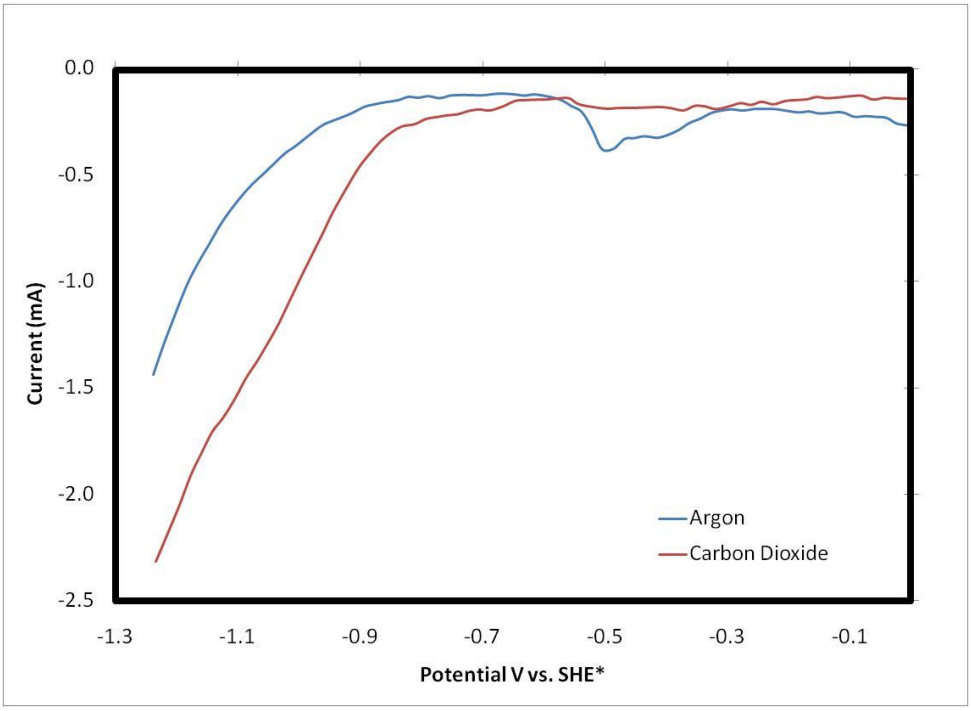

Figure 4.11: CV of CO_2 Reduction on Silver Nanopowder in 18mol% EMIM BF_4 in Water.

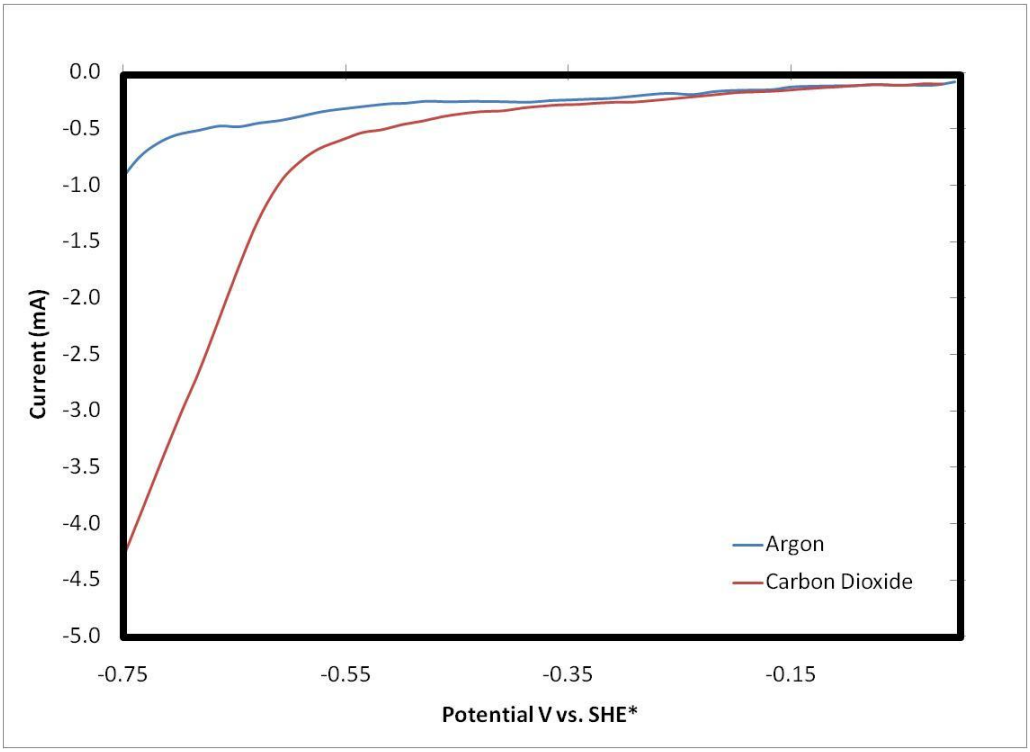

Figure 4.12: CV of CO_2 Reduction on Platinum Black in 18mol% EMIM BF_4 in Water.

The first clear point to be made between Figures 4.10, 4.11, and 4.12 is that the current using the gold electrode is the lowest, owing to the surface area of the gold electrode compared to the silver or platinum. Because of this surface area deficiency, we see a full faradic peak with amplitude of about -500µA around -500mV vs. SHE. The same limitations are not seen in the silver system and in the platinum system, but rather, there are two reduction regions evident by the changing slope of the reduction curve. In silver, the shallower region of CO_2 reduction is extended to approximately -900mV vs. SHE before the slope of the I-V curve increases (presumably due to rapid water reduction). As would be expected, this region occurs at less negative potentials when platinum is used as the cathode. Figure 4.12 shows that when platinum is used as the

cathode, this transition of dominant CO_2 conversion to dominant water reduction occurs near -600mV. The tradeoff is that platinum is able to produce a larger current compared to the silver. This result is both expected and reasonable as the overpotential for water reduction higher on silver compared to platinum. Depending on the design of the electrochemical cell, it may be desirable to utilize either a platinum catalyst (for slow steady production of CO at low overpotentials) or silver catalyst (for limited water reduction at slightly larger overpotentials). The use of both silver and platinum cathodes under steady state electrolysis conditions is discussed later in this work in Section 4.2.

4.1.6 CO Oxidation from Platinum Surface

Hori et al. explains the importance of verifying the species formed in CO_2 reduction reactions and not simply assuming the formation of a product based on a difference current. In conjunction with using optical techniques, this study wishes to probe the species bound to the catalyst surface by performing a series of oxidation experiments. Additionally, by varying the amount of time that the cathode is held at a reducing polarization, more kinetic information can be derived from the experiment. Figure 4.13 below is an example of this study. A solution of EMIM BF_4 and water (1M) had both CO_2 and CO bubbled through while the platinum black cathode was held at -600mV vs. SHE for 10 minutes. In the case of CO_2 saturation, this has shown to be a potential sufficient for CO_2 reduction; in the case of a CO saturated solution, this polarization should encourage the adsorption of CO onto the platinum surface, and perhaps further reduction on the surface. After ten minutes, the potential was swept from -600mV to +2000mV at a scan rate of 5mV/s. Similarities in the oxidation profiles

between CO_2 and CO saturated solutions can provide evidence that the reduced species is in fact CO.

Figure 4.13 shows the result of this experiment, and also provides the same experiment done in pure EMIM BF_4 and EMIM BF_4 with 1M water as a control experiment. In CO_2 saturated solution we see two predominant peaks, first a broad peak starting near the reducing potential; because of its position, it is presumed that this is a simple one electron transfer from an electron rich CO_2 species or reduced species to a less reduced form, for example:

$$CO_3^{2-} + CO \rightarrow e^- + CO_2 + CO_2^{-*} \tag{4.4}$$

It is unlikely that this initial peak is due to the reduction of CO for two reasons (i) it is expected that CO oxidation occur at significantly higher potentials (ii) this peak is much less dominant in the CO saturated solution.

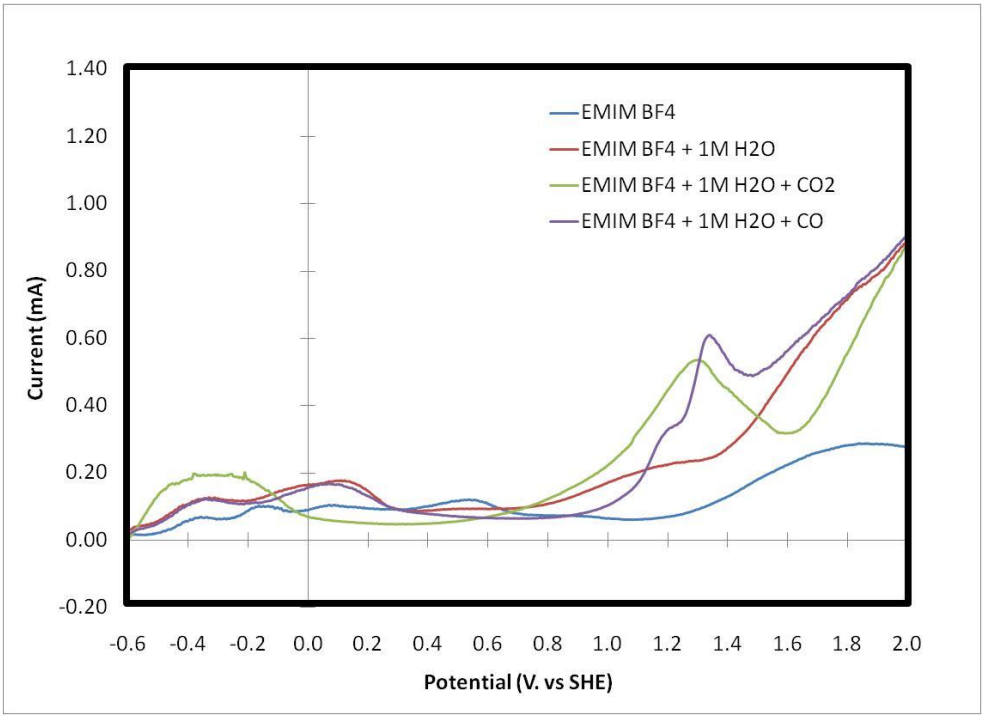

Figure 4.13: Minute Potential Hold at -600mV on Pt; Release 5mV/s.

In the region of 0 to +600mV vs. SHE, there appear to be small amounts of solvent related oxidation processes occuring. These oxidation steps appear to be associated the oxidation of hydrogen gas on the surface (i.e. $H_2 \rightarrow 2e^- + 2H^+$). This is is because (i) the peak begins slightly negative of 0 vs. SHE (representing the hydrogen overvoltage) and (ii) this peak is not present in the pure EMIM BF_4 system. Finally, the most dominant feature of this scan is the large oxidation peak beginning at ca. 1V and peaking near 1.3V vs. SHE. This peak likely represents the oxidation of CO back to CO_2. This process occurs around 700mV in aqueous systems, but appears to require a much stronger oxidizing potential in order to occur in the ionic liquid system. As per the hypothesis of this paper, the reduction potential is less negative due to the stabilization of the reduced CO_2 species and intermediates; the flip side to this is that if they are

stabilized, it is expected that a larger oxidizing potential would be required in order to regenerate adsorbed CO_2 on the surface. In summary, it is believed that the agreement between these two scans represents supporting evidence that CO is on the surface of the platinum electrode in using this EMIM BF_4-H_2O system.

A similar experiment was conducted in the absence of water in order to determine the importance of a small amount of water in the system on both the oxidation and reduction properties of the system. The potential was held at the value indicated for 10 min, and again swept forward to 2V at a rate of 5mV/s. Figure 4.14 below shows the potential dependence on this experiment when only 80mM (background) water is present in the system.

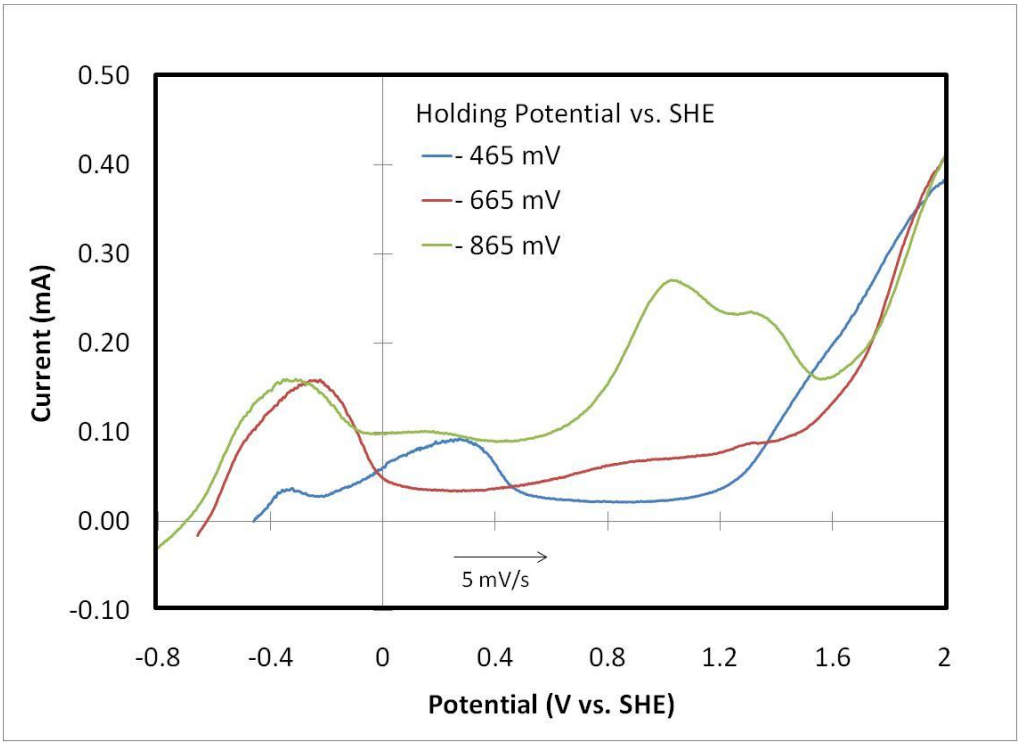

Figure 4.14: Reduced-CO_2 Oxidation at Variable Potentials.

When water is present in lower quantities, it appears to be much more difficult to generate CO on the surface as its oxidation peak does not appear until the reducing potential is near -865mV. This result is also suggested by Figure 4.14 above. The intermediate species, however, are still formed at potentials around -665mV, and at a low reducing potential, -465mV, only a small amount of intermediate species is observed and the more dominant oxidation peak is the splitting of adsorbed H_2 to 2 H. As more reduced species are produced (at lower potentials) the surface becomes covered with reduced CO_2 species and the hydrogen oxidation peak disappears due to inadequate surface site for the reduction of water. Figure 4.14 represents the nature of the competition between different surface reactions. With water concentrations between 80-500mM, and at potentials between -500mV and -900mV, on platinum, it appears that hydrogen generation exists at an optimal amount on the surface; not so much as to suppress CO_2 reduction and overwhelming the surface with hydrogen, and not so little as to make the removal of CO from the surface difficult.

4.1.7 Time Dependence of Oxidation Processes on a Pt Cathode

It is of kinetic interest to investigate the dependence of the oxidation profile on the time that the cathode was held at the reducing potential. The setup of this experiment was identical to the experiment summarized by Figures 4.13 and 4.14 with the holding time and potential variant. Figure 4.15 below shows the oxidation profile of a Pt cathode held at -565mV vs. SHE for 1, 5, and 10 minutes.

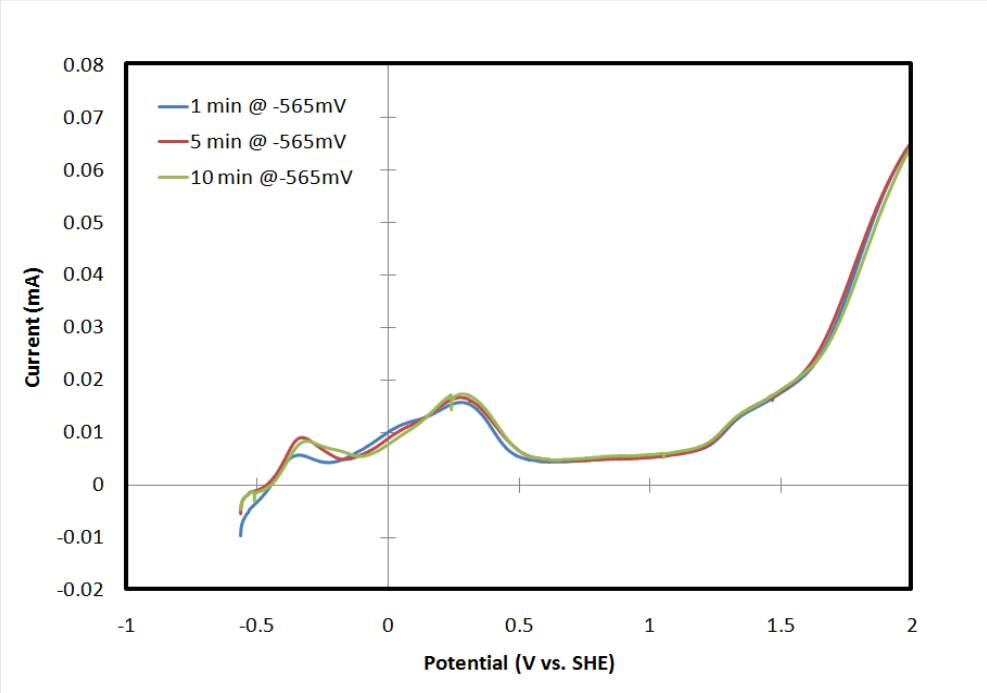

Figure 4.15: Oxidation Profile of CO_2 Saturated System Held at -565mV for 1, 5, and 10 Minutes.

What appears to be occurring at -565mV is the reduction of CO_2 in small amounts as evident by the oxidation peaks at -400mV and +1300mV. As discussed earlier, the oxidation peak at -400mV is likely due to the one electron oxidation of the CO_2^- intermediate back to CO_2, and/or the oxidation of CO_3^{2-} back to the CO_2^- intermediate as described by equation 4.4. Notice that the peak size of this initial oxidation appears to be time dependent, whereas the hydrogen oxidation peak and CO oxidation peak appear to be time independent.

Next, the potential of the cathode was held at -665mV vs. SHE for 1, 5, and 10 minutes. The major difference between this oxidation profile and the previous profile shown in Figure 4.15 is the apparent time dependence of both the intermediate oxidation peak (ca. -400mV) and the hydrogen oxidation peak (+250mV). Like other experiments

involving the competition between water and CO_2 on the platinum surface, this figure is very characteristic of this competitive process. Figure 4.16 shows that as the potentiostatic time is increased from 1 to 10 minutes, more and more CO_2 appears to be reduced on the surface at the expense of less hydrogen splitting. This is shown by the positive correlation between peak size and time for the CO_2^{-}/CO_3^{2-} process and the inverse correlation between peak size and time for the hydrogen splitting peak. At such low potentials, it appears that there is still no time dependence for the size of the CO oxidation peak back to CO_2. It is important to remind the reader that the CO oxidation peak on Pt, usually found at ca. +800mV is found at higher potential due to the large interaction parameter between CO_2/reduced-CO_2 species and the ionic liquid.

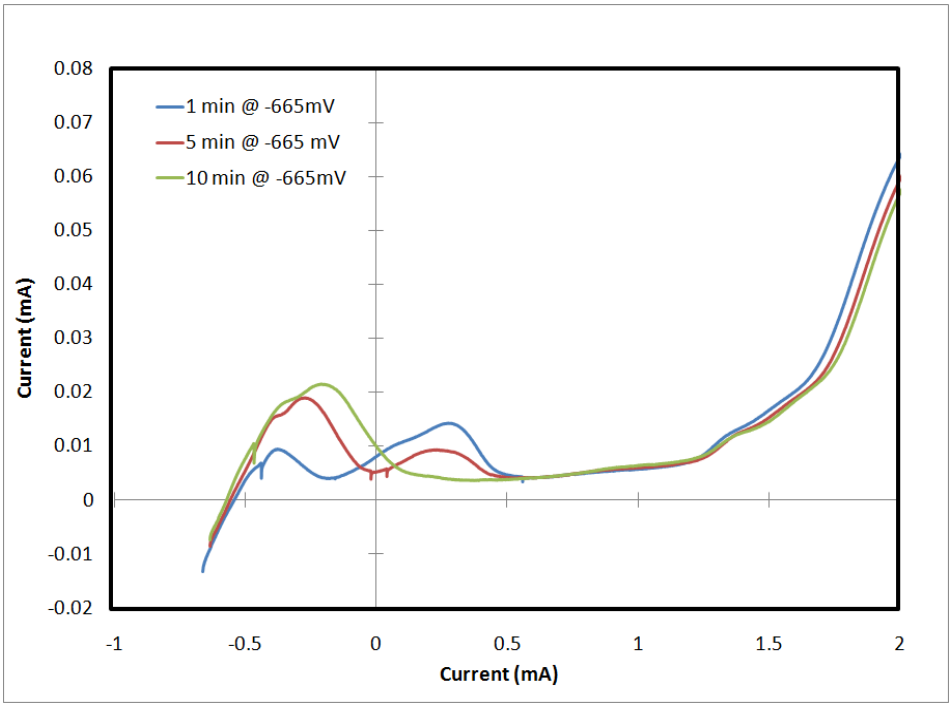

Figure 4.16: Oxidation Profile of CO_2 Saturated System Held at -665mV for 1, 5, and 10 Minutes.

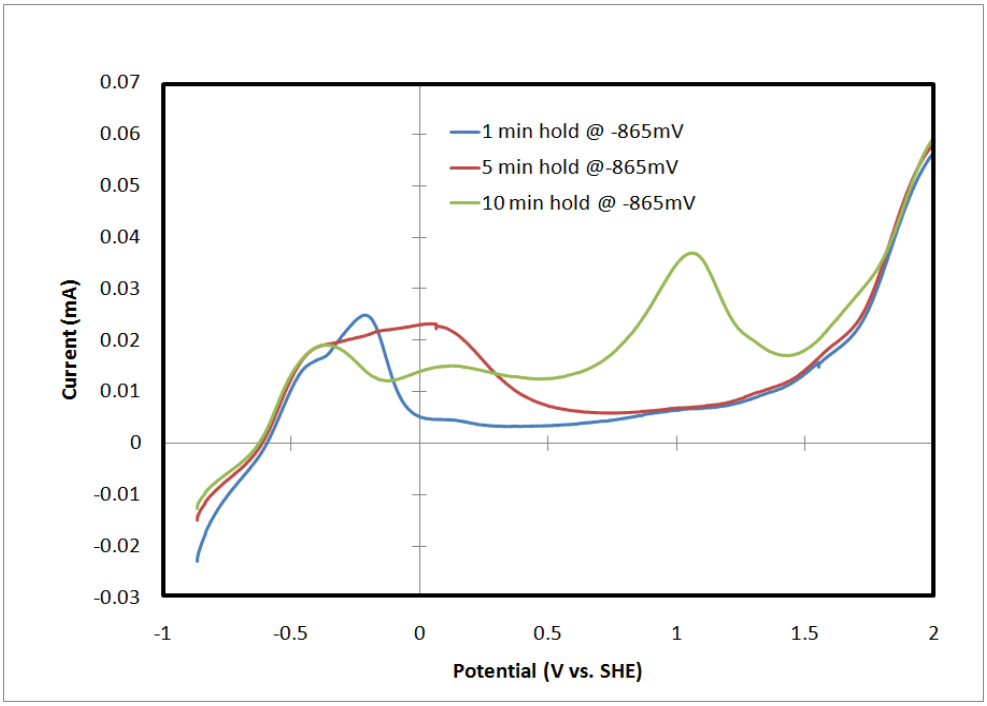

Figure 4.17: Oxidation Profile of CO_2 Saturated System Held at -865mV for 1, 5, and 10 Minutes.

Finally, we wish to look at the time-dependent oxidation profile under CO_2 reducing conditions at -865mV vs. SHE. At this potential, it appears that many more processes are occurring on the electrode surface, making the figure harder to de-convolute; however, the same major features from Figures 4.16 and 4.17 are still present. At this lower potential, we see little to no time dependence on the initial oxidation peak (CO_2^-/CO_3^{2-}) . As the time is increased from 1 to 5 to 10 minutes, we see a broadening of this initial peak into the hydrogen region, perhaps indicating a significant increase in the amount of reduced intermediate on the surface compared to the other two potentials. We also see that at 10 minutes under this condition, much of the intermediate is converted to CO on the surface as evident by the large faradaic peak around 1200mV. As shown earlier in Figure 4.13, this peak is due to the oxidation of CO back to CO_2.

In summary, we see the potential and time dependence of CO_2 reduction in EMIM BF_4 on the nature of the species found electrochemically on the surface. It will be shown in later sections that these results are also consistent in experiments that are not transport limited, and that the CO and H_2 on the surface suggested by these oxidation experiments are found to be continuously produced in an CO_2 electrolyzer.

4.1.8 CO_2 Interaction Suggested by CO_2 Diffusion Measurements

The Stokes-Einstein equation (Equation 4.5) describes the relationship between a molecule of hydrodynamic radius, R, in a liquid of viscosity, η, at temperature, T, to the molecules' diffusion coefficient, D.

$$D = \frac{kT}{6\pi mR} \tag{4.5}$$

Using the model parameters found below in Table 4.1 and Equation 4.5, it would be expected that CO_2 has a diffusion coefficient of 1.3×10^{-11} m^2/s in EMIM BF_4 at 25C.

One may also infer the diffusivity of an electrochemically reacting species (in this case, CO_2 and/or its intermediates) by fitting to a model that determines the diffusivity at a disc electrode held at a constant potential[1]. While this model is not an exact analytical solution, it has been used by Richard Compton, a known leader in Ionic Liquid chemistry, as well as other well known electrochemists. The steady state current is related to the diffusivity of the reacting species via equation 4.6 below.

$$|I(t)| = A + Bt^{-1/2} + 0.2732A\exp\left(-0.3911\pi^{1/2}B \Big/ At^{1/2}\right) \tag{4.6}$$

The steady state diffusivity comes from the fitted "A" parameter by:

$$A = \pi FancD \tag{4.7}$$

Electrochemically, the diffusivity of CO_2 was measured to be at most $3.02x10^{-12}$ m^2/s. This is an order of magnitude difference between the expected diffusivity based on viscosity effects. The electrochemically inferred diffusivity suggests that there is an additional interaction parameter between CO_2 and EMIM BF_4.This conclusion is consistent with both this study and many other studies owing to the strong intra- and inter- molecular interactions (coulombic and hydrogen bonding) observed in ionic liquids.

Table 4.1: *Potentiostatic Diffusivity Model Parameters*.

	Constants		
		Value	**Unit**
	C	1.00E+03	[mol/m3]
(electrode rad.)	**a**	1.56E-03	[m]
	n	2	[1]
	F	96485	[As/mol]
	π	3.14E+00	[1]
	π ^(1/2)	1.772484	[1]
	k	1.38E-23	[J/K]
	T	298.15	[K]
(CO2 rad.)	**r**	5.50E-10	[m]
(EMIM BF_4) @ 25C	**η**	0.0306	[Pa S]

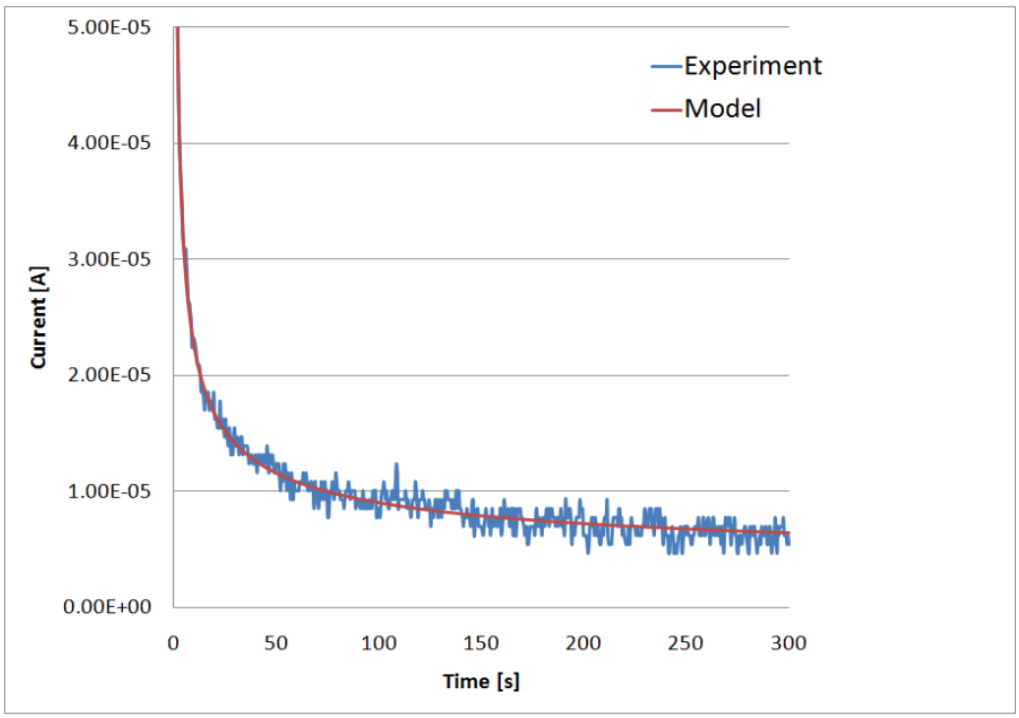

Figure 4.18: Model vs. Fit for Potentiostatic Reduction of CO_2 in EMIM BF_4.

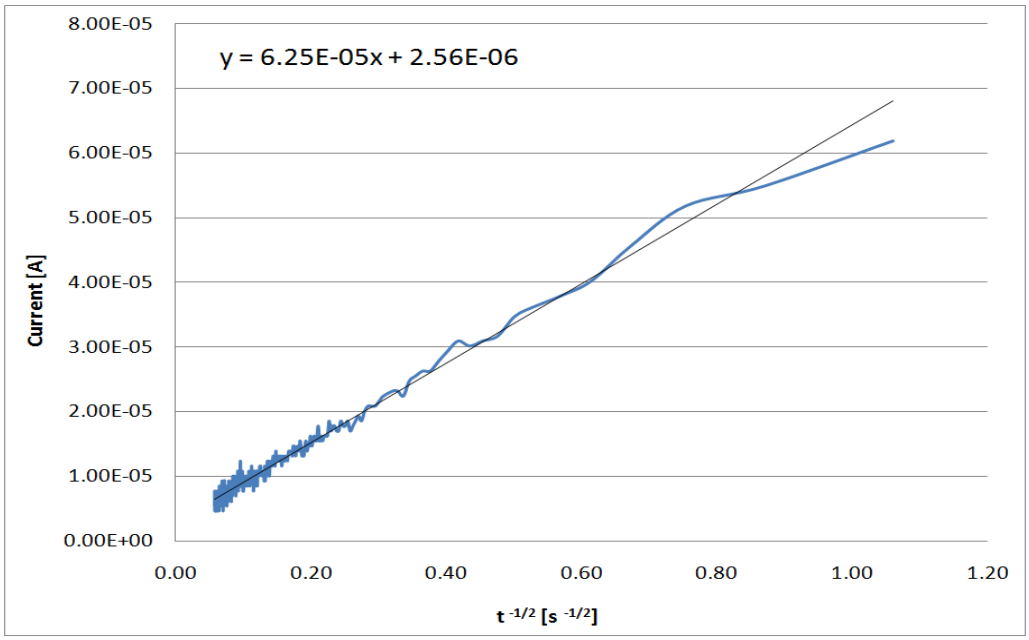

Figure 4.19: Nonlinear Model Fit to Terms 1 and 2 in Equation 4.6.

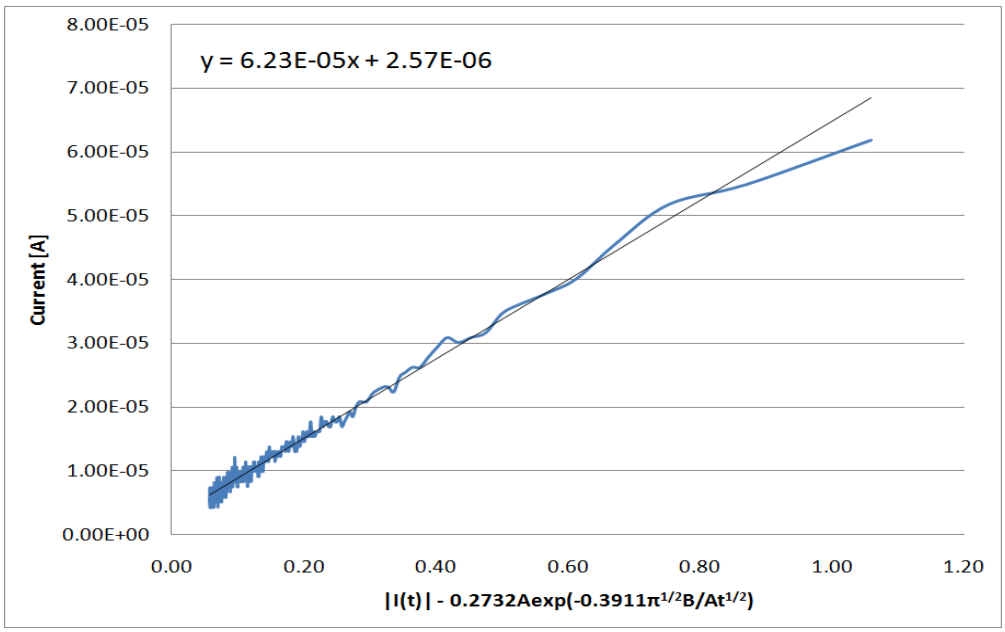

Figure 4.20: Nonlinear Model Fit to Term 3 in Equation 4.6.

4.2 Continuous CO_2 Reduction in an Electrolyzer

All of the experiments described above are in a mass transfer limited condition. It is the goal of this project to use the data acquired from experiments conducted in our electrochemical cells for use in the design of a continuous flow CO_2 electrolyzer. In this study, the use of both platinum and silver cathodes (at the same loading) were investigated. Table 4.1 below shows the cell operating conditions for both cathode varieties. In both cases, the anode was made of platinum black deposited on carbon paper (similar to the cathodes) except the loading was only 2mg/cm^2.

Table 4.2: Reactor Operating Conditions.

Platinum (5mg/cm^2) Cathode	**Silver (5mg/cm^2) Cathode**
Cell Temperature: 110C	Cell Temperature: 25C
Gas Phase: 100% CO_2	Gas Phase: 100% CO_2
Liquid Phase: EMIM BF_4 + 500mM Water	Liquid Phase: 18%mol EMIM BF_4 in Water
Cathode Potential: -0.75V vs. SHE	Cathode Potential: -0.85V vs. SHE
Gas Flow Rate: 2.5 sccm	Gas Flow Rate: 2.5sccm
Liquid Flow Rate: 1ml/min	Liquid Flow Rate: 0.5ml/min

In both cases, the liquid stream was fed into a scintillation vial with the reference electrode. The reference electrode was hooked up to both the cathode and the anode in order to monitor the polarization of the electrodes independently. The gas stream was fed

directly into an SRI GC where 100µl samples were fed into a 6’ Molecular Sieve 5A column and then to a TCD detector. The operating conditions for the GC system are found below in Table 4.2.

Table 4.3: GC Operating Conditions.

Operator	**Setpoint**
TCD Detector Temperature	110C
GC Column Temperature	100C
Carrier Gas Pressure	14psi
TCD current	125mA

The electrolysis cell was constructed in layers shown below in Figure 4.21. The gas channel was made of aluminum. In direct contact with the gas channel is a piece of carbon paper with a cross section just a few millimeters larger than the channel opening. This piece of carbon paper has 10mg of Pt (or Ag) nanopowder painted on. Beneath the cathode is a PTFE layer that serves as a liquid channel; this layer also electrically isolates the cathode from the anode. Beneath the PTFE layer is the anode (facing up into the liquid channel) where there was 4mg of Pt black painted on the side facing the liquid channel. Beneath the anode was another aluminum piece used for both structural integrity and as an anodic current collector. In order to prevent electrical connection between the bolts and two aluminum layers, a PTFE layer is placed beneath the anode current collector (not shown), and all of the bolts have a layer of PTFE tubing on the outside of their threads to prevent short circuiting within the device.

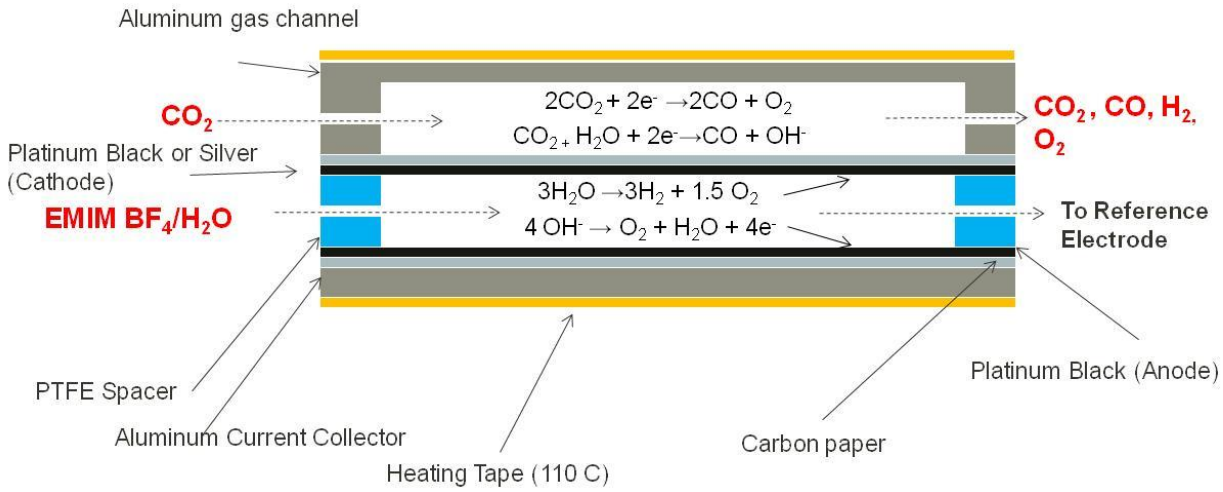

Figure 4.21: Schematic of CO_2 Electrolysis Cell with Dominant Reactions.

This device has proven to be useful for several reasons, including: (1) small distance between the cathode and anode leading to only small solution resistances (2) fast transport and accessibility of CO_2 to the cathode through the porous conductive carbon fibers (3) solvent flexibility and byproduct removal as a result of the flowing liquid stream (4) rapid heat conduction and equilibration and (5) ability to directly connect the cell to a reference electrode and gas chromatogram.

Figure 4.22 below shows the composition of the exit gas stream from the electrolyzer when the cathode is made of platinum black. Notice that both hydrogen and CO are present in significant amounts in the product stream. In this experiment, the cell was held at a potential of 2.25V, which polarizes the cathode to approximately -0.75V vs. SHE. This cell was held at this potential for 4 hours (at 110C) at which point no more CO was detected in the exit stream. This result is most likely due to the crossover of ionic liquid through the carbon paper layer into the gas channel. If this is happening, a layer of

ionic liquid would form on the topside of the carbon paper preventing the CO_2 reactant from reaching the cathode catalyst; it is at this point that we consider the reactor to be flooded and no product is observed.

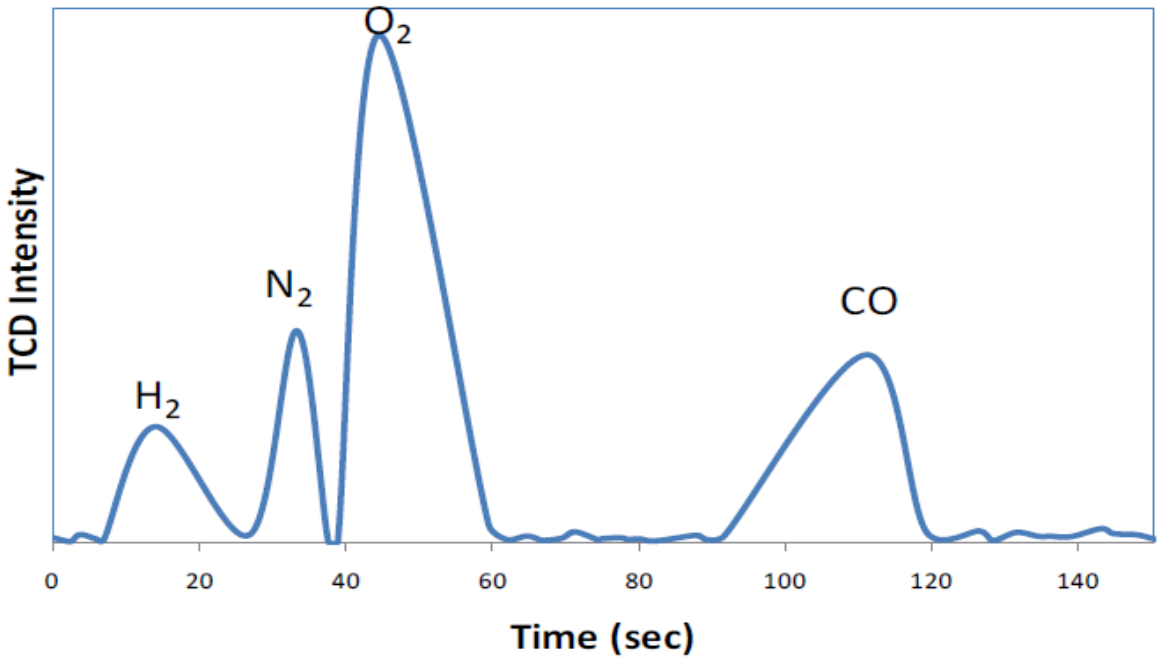

Figure 4.22: GC Spectra of Gas Phase Products for CO_2 Electrolysis Cell with Pt Cathode.

Note also from Figure 4.22 that we see hydrogen in the exit stream due to the presence of 500mM water in the liquid phase feed stream; the presence of hydrogen gas under these conditions is consistent with data observed in the transport limited electrochemical cell. Finally, we also observe an increase in the oxygen peak relative to background levels. The appearance of oxygen in the exit gas stream is a result of hydroxide ion oxidation at the anode and water reduction at the cathode. Due to the small

gap between the cathode and anode, it is certainly possible that the oxygen produced at the anode is able to diffuse into the gas stream.

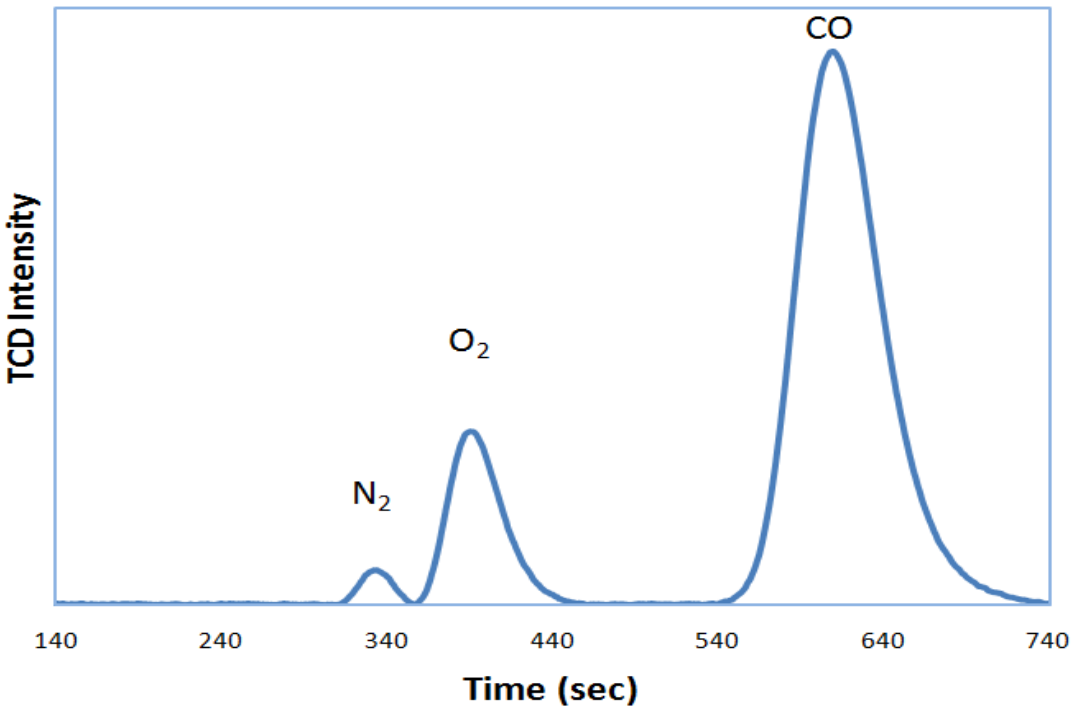

Figure 4.23: GC Spectra of Gas Phase Products for CO2 Electrolysis Cell with Pt Cathode

Figure 4.23 above shows the GC spectrum of the gas phase products with a silver cathode. Under these circumstances, we are using only 18%mol EMIM BF_4 (the remaining 82%mol is water); however, we still do not see the presence of the hydrogen peak. This is an excellent result because this means that even under dilute conditions, we can selectively form CO at high faradaic efficiencies using a silver cathode. This is not to say that hydrogen is not adsorbed on the surface, but rather the hydrogen evolution reaction is not taking place at a significant rate under these experimental conditions. Figure 4.23 suggests that as this project pushes forward to optimize our electrodes, silver

will be a good place to start as it is much cheaper that platinum, and provides us with the proper selectivity to CO (consistent with aqueous phase data). The absence of hydrogen in this GC spectrum could be due to two reasons (1) inhibition of hydrogen evolution by imidazole on the silver surface and (2) larger overpotential of hydrogen evolution (compared to Pt) on silver.

CHAPTER 5

SPECTROSCOPIC RESULTS AND DISCUSSION

5.1 Sum Frequency Generation (SFG) of CO_2 Reduction on a Platinum Cathode

We used a recently developed compact broadband multiplex Sum Frequency Generation Spectroscopy (SFG) apparatus [23] to determine whether the EMIM-BF_4-$(CO_2)^-$ complex forms in the ionic liquid EMIM BF_4, and to determine the potential for the formation of the complex. Figure 5.1 shows a series of SFG spectra taken during CO_2 electrolysis in EMIM-BF_4. At cathode potentials more positive than +0.04V with respect to a standard hydrogen electrode (SHE) we observe only a broad peak due to non-resonant scattering [24, 25] which represents the spectrum of IR pulses from the SFG apparatus. However, as the cathode potential moves more negative, a new narrow peak appears at 2340 cm^{-1}. Simultaneously, cyclic voltammetry(CV) in Figure 5.2 shows that current is flowing into the solution. We also find that the SFG peaks associated with the EMIM species increase as shown in Figure 5.3.

We attribute the peak to the formation of an EMIM-BF_4-CO_2^- complex via the reaction

$$\text{EMIM-BF}_4 + CO_2 + e^- \rightarrow \text{EMIM-BF}_4\text{-}CO_2^- \qquad (5.1)$$

Figure 5.1 shows that the new species has a stretching frequency of 2348 cm^{-1}. By comparison, gas phase CO_2 shows a stretching frequency of 2396 cm^{-1} [26]. Thus, it appears that new species contains CO_2. The species cannot simply be an adsorbed CO_2 molecule, however. For CO_2 to be SFG-active, it must be present in an environment that imbues both IR and Raman activity to its vibrational transitions and the environment must exhibit noncentrosymmetric order on scales comparable to a visible wavelength.

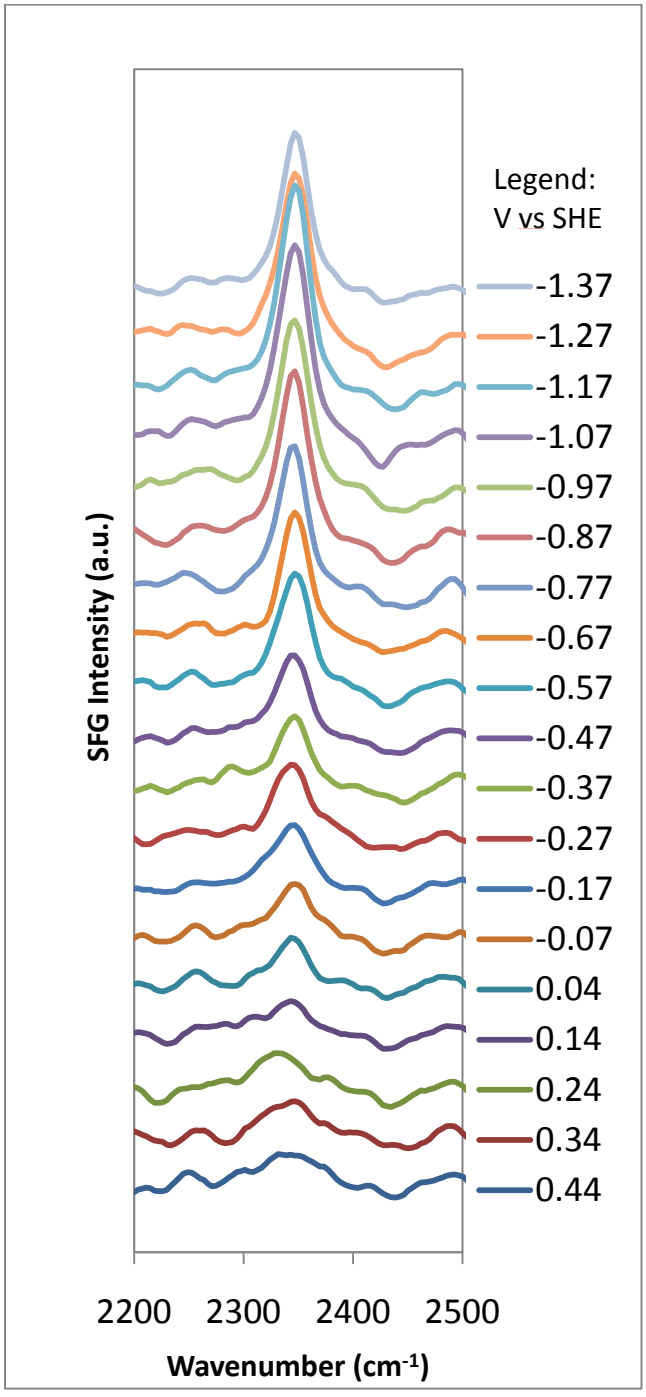

Figure 5.1: SFG Signal of Asymmetric CO_2 Stretch from CO_2—EMIM Complex.

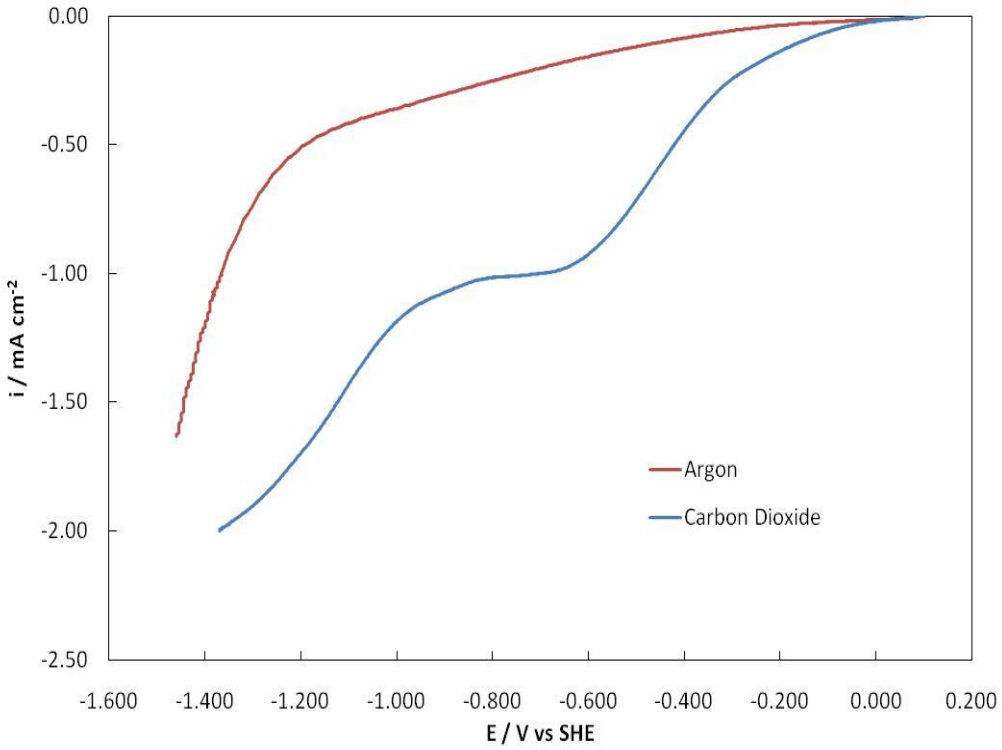

Figure 5.2: LSV taken in-situ with SFG Experiment.

The frequency of the vibrational band at 2348 cm^{-1} can be attributed to antisymmetric CO_2 stretching vibration. Note that the free CO_2 molecule has inversion symmetry, the Raman polarizability α_q therefore vanishes for the antisymmetric stretching vibration. As a result, vibrational bands at 2396 and 2341 cm^{-1} of free undistorted CO_2 molecules [26] and CO_2 [27, 28] in liquid electrolytes, respectively, are not observed in Raman and is not expected in SFG spectra. However, our SFG spectra of polycrystalline Pt and Au electrodes in contact with CO_2 saturated EMIM-BF_4 clearly show an intense vibrational band of CO_2 at 2348 cm^{-1} which is very close to the vibrational band of CO_2 in liquids previously reported [27, 28]. The existence of this band in SFG spectra reveals that the majority of interfacial CO_2 molecules exhibit

physical and chemical properties that are very different from gaseous CO_2 or CO_2 in the bulk electrolyte. A conceivable possibility is that the CO_2 band arises from CO_2 linearly adsorbed onto the Pt surface and with the molecular axis perpendicular to the electrode surface. Other adsorption geometries e. g. a bidendate configuration with two oxygen binding to the metal surface are unlikely since they would lead to significantly red shifted band at in frequencies <1700 cm^{-1}[26, 29, 30]. The near gas phase value of the stretching vibration observed in our spectra (Fig. 4.1) suggests weak interactions with the metal substrate and a physisorbed species which must be related to a CO_2 species parallel to the surface [26, 30]. The latter has negligible dynamic dipole moments and leads to inactive SFG transition only. A monodentate configuration is therefore highly unlikely and must be disregarded as well.

It is more likely that the interfacial CO_2 forms a complex with the EMIM cation that lifts the inversion symmetry of the CO_2 molecule and gives rise to a SFG and possibly Raman active band due to antisymmetric stretching vibrations. Strong support for this hypothesis comes from ab-inito calculations of CO_2 complexes with aromatic [29] or imidazolium rings[31]. In particular Bhargava et al. [31] report that in a BMIM-PF_6 ionic liquid the CO_2 forms a complex with the BMIM cations via weak hydrogen bonds. CO_2 attached to the BMIM cation differs from its linear form and lifts the degeneracy of the bending mode [31]. Furthermore, Besnard et al. report for a CO_2-C_6F_6 dimer that the Raman polarizibilies of the antisymmetric CO_2 stretch are changed to non-zero values, allowing for a weakly active Raman and SFG transitions at 2414 cm^{-1}[29]. It is important to note that the differences in frequency between the CO_2-C_6F_6 dimer and the CO_2 frequency observed in our SFG experiments are possibly due to the collective

interactions of the CO_2 and the cations and anions of the IL. The latter have not been considered in the calculations and known to cause frequency shifts of ~55 cm^{-1} e.g. for CO_2 in liquids with and gas phase CO_2 without interactions.

CO_2 usually lies flat on metals, so CO_2 adsorbed on a metal surface would be SFG-inactive. However if CO_2 were attached or complexed with an imidazole ring, CO_2 vibrations would be both IR and Raman-active [27]. If the complexes were interfacial, and especially if oriented by an electric field, strong SFG-activity would be observed. We observe a stretching frequency of 2348 cm^{-1} compared to 2338 cm^{-1} for CO_2 bound to BMIM [41]. These results provide strong evidence that the CO_2 is forming a complex with the EMIM-BF_4.

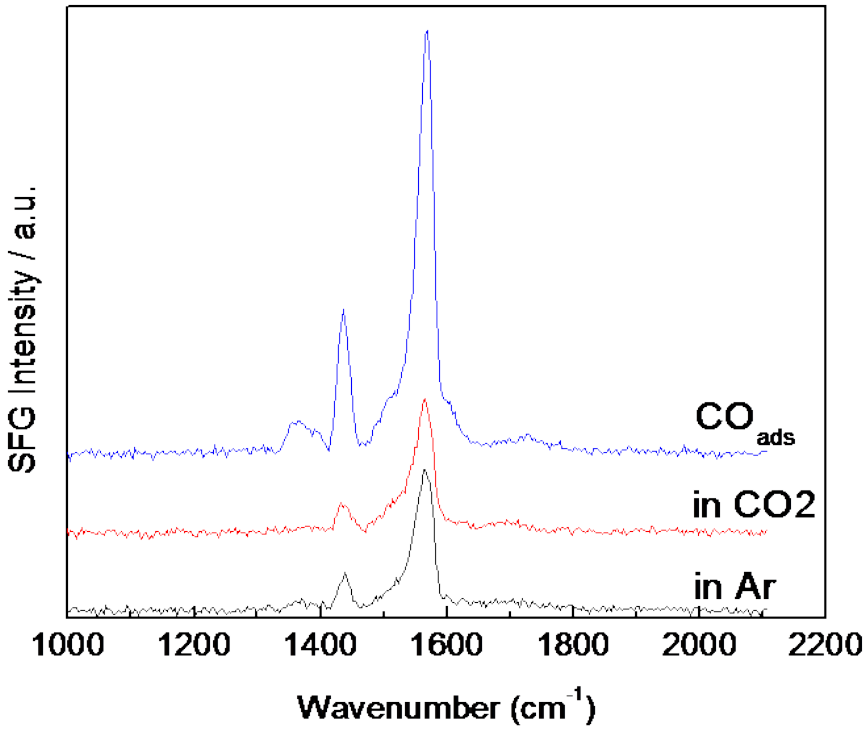

Figure 5.3: SFG of Imidazole Ring Breathing Vibration Mode.

We identify the complex as having a negative charge (i.e. EMIM-BF_4-CO_2^-) since the complex only forms at potentials where electrons are being added to the solution (see Figure 5.2).

It is useful to compare the results in Figure 5.1 to the previous results. Lamy et al found that the equilibrium potential for $(CO_2)^-$ formation is -2.46 V in Dimethylformamide (DMF). Metals lower the needed potential, but still, Chandrasekaran and Bockris suggested that in acetonitrile doped with tetraammonium $(CO_2)^-$ does not start to form on platinum until the potential is below -0.8 V with respect to SHE. Notice that we observe what we interpret as being a negatively charged CO_2 complex at -0.14 V with respect to SHE. We also observe significant current in this potential range. Our conclusion is that the EMIM-BF_4-$(CO_2)^-$ complex can form near zero with respect to SHE. This compares to -0.8V in the absence of the ionic liquid. Evidently, the ionic liquid is stabilizing the $(CO_2)^-$ as indicated in Figure 5.1.
The next question is whether the $(CO_2)^-$ is reactive or whether it has been stabilized so much that it became unreactive. SFG was also used to examine that possibility. Figure 5.4 shows the CO region of the spectrum during experiments similar to those in Figure 5.1. There is a broad peak due to the non-resonant susceptability and a narrower vibrational band due to adsorbed CO. The CO transition starts at 2050 cm^{-1}, shifts down to 2040 cm^{-1} due to the Stark effect [28, 29]. In data not shown, it shifts up again due to dipole interactions as the CO coverage increases [30, 33]. All of these behaviors are as expected for CO formation on platinum.

There are some important details of this experiment. The EMIM-BF_4 contains about 80 mmol water. Thus, CO can form by one of two reactions

$$2\ CO_2 + 2e^- \rightarrow 2\ CO + O_2^{2-} \quad (5.1)$$

$$CO_2 + H_2O\ 2e^- \rightarrow CO + 2OH^- \quad (5.2)$$

Also, the design of our SFG cell is such that the formation of CO is mass transfer limited. Generally, the platinum electrode sits at about 50 microns away from a CaF_2 window and the SFG is done at a spot near the center of the electrode. In order for reaction to occur, the CO_2 and water need to diffuse down the space between the electrode and the window. Experimentally, we found that if we held the electrode potential fixed at for example -0.5 V, the CO_2 and water are used up before they get to the center of the electrode. Thus one would not detect significant CO buildup in SFG at a fixed potential.

One can observe CO buildup if one does the experiment in a cyclic mode, where one holds the electrode at the open cell potential, to allow the reactants to diffuse to the center of the electrode, and then cycle the electrode down to some negative potential (e.g. -0.25 V) and allow the species to react.

Figure 5.4 shows CO buildup is observed whenever the electrode was repetitively cycled down to a potential of -0.25 V with respect to SHE. By comparison, CO buildup on platinum is not normally observed until the potential is below -1.1 V [34]. Thus, it appears that the conversion of CO_2 to CO can occur at much less negative potentials in our system than has been observed previously.

We have also done similar experiments on gold. We observe the formation of the EMIM-BF_4-$(CO_2)^-$ complex on gold. The data is given in Figure S4. However, we do not observe CO formation on gold.

We now address the different SFG intensities of CO_2 vibrational bands at Au and Pt surfaces in contact with EMIM-BF_4. The intensity of vibrational bands at metal interfaces strongly depends on the net dipolar orientation of the molecules at the interface. Consequently, the orientation of the ionic liquid cations at Pt and Au interfaces and their complexes with CO_2 molecules determines the strength of the associated vibrational bands. It is reasonable to conclude that the interfacial layer of the IL is much more ordered in Au than on Pt surfaces and gives rise to a more intense CO_2 band.

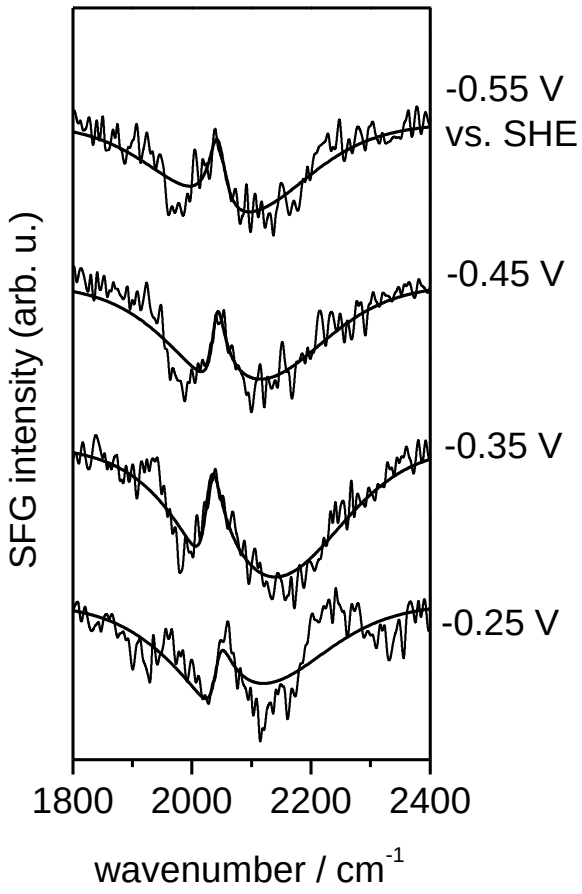

Figure 5.4: SFG Spectra (inverted) of CO Region at CO_2 Reducing Potential.

CHAPTER 6

CONCLUSIONS

This work has shown that the Room Temperature Ionic Liquid (RTIL) 1-ethyl-3-methylimidazolium tetrafluoroborate (EMIM BF_4) has a many favorable characteristics that can enable the reduction of CO_2 at less negative potentials compared to previous work, as well as at low temperatures. It was shown through electrochemical oxidation experiments, potentiostatic diffusion modeling, and in-situ Sum-Frequency-Generation (SFG) Spectroscopy that there is a strong stabilizing interaction between the CO_2^- anion radical and the ionic liquid. From this same work, it is also shown that there is an increased interaction parameter between the EMIM BF_4 and the neutral CO_2 and CO species. The electrochemistry (oxidation profiles) and spectroscopy (SFG) performed in this work has shown that CO_2 is largely reduced to CO on a platinum cathode.

This work has shown the importance of water concentration on the conversion of CO_2 to CO. Too little water makes it difficult for CO to oxidize off of the surface and leaves only non-aqueous reduction pathways, while too much water encourages hydrogen formation on the surface thereby lowering the faradaic efficiency of CO production by raising the overpotential for CO_2 conversion.

Furthermore, it was shown that this electrochemistry can be applied to a continuous flow CO_2 electrolyzer to which CO and H_2 (depending on the cathode metal) can be continuously produced in the gas phase at low temperature and potential. It is the future goal of this research to optimize the electrode design, in order to work on scaling up the electrolyzer to produce larger volumes of synthesis gas product. This optimization will come by clever design of the gas diffusion layer support, electrode metal, as well as

the binder chosen to adhere the electrode metal to the support. Finally, future work on this project will make advances in revealing the CO_2 conversion mechanism taking place on the surface so we can better quantify the thermodynamics and kinetics of this new system.

REFERENCES

1. Hori, Y., Modern Aspects of Electrochemistry, 2008. **42**: p. 89-189.
2. Halmann, M.M., 1993, Rehovot, Israel: CRC Press.
3. Pinset, B.R.W., L. Pearson, and F.J.W. Roughton,. Trans. Faraday Soc. , 1956. **52**: p. 1512.
4. Azuma, M., et al., Journal of the Electrochemical Society, 1990. **137**(6): p. 1772-8.
5. Jitaru, M., et al., Journal of Applied Electrochemistry, 1997. **27**(8): p. 875-889.
6. Kita, H. and T. Kurisu, Journal of the Research Institute for Catalysis, Hokkaido University, 1973. **21**(3): p. 200-46.
7. Schwarz, H.A. and R.W. Dodson, The Journal of Physical Chemistry, 1989. **93**(1): p. 409-414.
8. Surdhar, P.S., S.P. Mezyk, and D.A. Armstrong, The Journal of Physical Chemistry, 1989. **93**(8): p. 3360-3363.
9. Chaplin, R.P.S. and A.A. Wragg, Journal of Applied Electrochemistry, 2003. **33**(12): p. 1107-1123.
10. Gennaro, A., et al. Journal of the American Chemical Society, 1996. **118**(30): p. 7190-7196.
11. Tomita, Y., et al., J. Electrochem. Soc. , 2000. **147**.
12. Fischer, J., T. Lehmann, and E. Heitz,. Journal of Applied Electrochemistry, 1981. **11**(6): p. 743-750.
13. Amatore, C. and J.M. Saveant, Journal of the American Chemical Society, 1981. **103**(17): p. 5021-5023.
14. Eggins, B.R. and J. McNeill, Journal of Electroanalytical Chemistry, 1983. **148**(1): p. 17-24.
15. Aylmer-Kelly, A.W.B., et al., Faraday Disc. Chem. Soc., 1973. **56**: p. 96.
16. Silvester, D.S. and R.G. Compton,. Z. Phys. Chem., 2006. **220**: p. 1247-1274.
17. Stoppa, A., et al., Journal of Chemical & Engineering Data, 2009.
18. Zigah, D., et al.. J. Phys. Chem B, 2009. **113**(7).
19. Finotello, A., et al., Industrial & Engineering Chemistry Research, 2007. **47**(10): p. 3453-3459.
20. Baldelli, S. Accounts of Chemical Research, 2008. **41**(3): p. 421-431.
21. Graves, A.D. and D. Inman, Journal of Electroanalytical Chemistry, 1970. **25**(3): p. 357-372.
22. Barrosse-Antle, L.E. and R.G. Compton. Chem. Comm., 2009: p. 3744–3746.
23. A. T. Bell. (US Department Of Energy, 2008), vol. US Department Of Energy report PNNL17712 http://www.sc.doe.gov/bes/reports/files/CAT_rpt.pdf.
24. N. S. Lewis, *Science (Washington, DC, U. S.)* **315**, 798 (2007).
25. N. S. Lewis, *ChemSusChem* **2**, 383 (2009).
26. N. S. Lewis, D. G. Nocera, *Proceedings of the National Academy of Sciences* **103**, 15729 (2006).
27. T. J. Meyer, *Nature (London, U. K.)* **451**, 778 (2008).

28. J. Tollefson, *Nature (London, U. K.)* **466**, 541 (2010).
29. Z. Chen *et al.*, *Proc. Natl. Acad. Sci. U. S. A., Early Ed.*, 1 (2010).
30. L. Hammarstrom, S. Hammes-Schiffer, *Acc. Chem. Res.* **42**, 1859 (2009).
31 B. Vincenzo, C. Alberto, V. Margherita, *ChemSusChem* **1**, 26 (2008).
32. Q. Yin *et al.*, *Science* **328**, 342 (April 16, 2010, 2010).
33. M. Gattrell, N. Gupta, A. Co, *J. Electroanal. Chem.* **594**, 1 (2006).
34. Y. Hori, *Mod. Aspects Electrochem.* **42**, 89 (2008).
35. D. M. Rakowski, D. L. Dubois, *Acc. Chem. Res.* **42**, 1974 (2009).
36. D. L. DuBois, *Encycl. Electrochem.* **7a**, 202 (2006).
37. J. O. M. Bockris, J. C. Wass, *J. Electrochem. Soc.* **136**, 2521 (1989).
38. K. Chandrasekaran, J. O. M. Bockris, *Surf. Sci.* **185**, 495 (1987).
39. R. I. Masel, *Chemical Kinetics and Catalysis*. (Wiley, NY NY, 2001).
40. A. S. Barnes *et al.*, *The Journal of Physical Chemistry C* **112**, 13709 (2008).
41. M. M. Islam, T. Ohsaka, *The Journal of Physical Chemistry C* **112**, 1269 (2008).
42 B.-H. Lim *et al.*, *Korean J. Chem. Eng.* **26**, 1130 (2009).
43. A. Maiti, *ChemSusChem* **2**, 628 (2009).
44. M. Shokouhi, M. Adibi, A. H. Jalili, M. Hosseini-Jenab, A. Mehdizadeh, *J. Chem. Eng. Data* **55**, 1663 (2010).
45. A. N. Soriano, B. T. Doma, Jr., M.-H. Li, *J. Chem. Eng. Data* **53**, 2550 (2008).
46. J. Tang, Y. Shen, M. Radosz, W. Sun, *Ind. Eng. Chem. Res.* **48**, 9113 (2009).
47. A. Lagutchev, A. Lozano, P. Mukherjee, S. A. Hambir, D. Dlott, *Spectrochim. Acta. A* **75**, 1289 (2010).
48. S. Baldelli, A. A. Gewirth, *Adv. Electrochem. Sci. Eng.* **9**, 163 (2006).
49. J. A. Carter, Z. Wang, D. D. Dlott, *Acc. Chem. Res.* **42**, 1343 (2009).
50. C. R. Bailey, *Nature (London, U. K.)* **123**, 410 (1929).
51. B. L. Bhargava, S. Balasubramanian, *J. Phys. Chem. B* **111**, 4477 (2007).
52. S. G. Kazarian, B. J. Briscoe, T. Welton, *Chemical Communications*, 2047 (2000).
53. S. C. Chang, X. Jiang, J. D. Roth, M. J. Weaver, *The Journal of Physical Chemistry* **95**, 5378 (1991).
54. X. Jiang, M. J. Weaver, *Surf. Sci.* **275**, 237 (1992).
55. W. F. Banholzer, R. I. Masel, *Surf. Sci.* **137**, 339 (1984).
56. C. W. Olsen, R. I. Masel, *Surf. Sci.* **201**, 444 (1988).
57. W. F. Banholzer, R. E. Parise, R. I. Masel, *Surf. Sci.* **155**, 653 (1985).
58. J. Wang, R. I. Masel, *Journal of Catalysis* **126**, 519 (1990).
59. D. T. Whipple, E. C. Finke, P. J. A. Kenis, *Electrochemical and Solid-State Letters* **13**, B109 (2010).
60. Y. O. Park, R. I. Masel, K. Stolt, *Surf. Sci.* **131**, L385 (1983).
61. Y. O. Park, W. F. Banholzer, R. I. Masel, *Applications of Surface Science (1977-1985)* **19**, 145 (1984).
62. M. J. Earle, K. R. Seddon, *ACS Symp. Ser.* **819**, 10 (2002).
63. E. I. Rogers *et al.*, *The Journal of Physical Chemistry C* **111**, 13957 (2007).
64. V. V. Pavlishchuk, A. W. Addison, *Inorganica Chimica Acta* **298**, 97 (2000).
65. H.-J. Freund, M. W. Roberts, *Surf. Sci. Rep.* **25**, 225 (1996).

66. P. A. Christensen, A. Hamnett, A. V. G. Muir, N. A. Freeman, *J. Electroanal. Chem.* **288**, 197 (1990).
67. A. Rodes, E. Pastor, T. Iwasita, **369**, 183 (1994).
68. M. Besnard, M. I. Cabaco, Y. Danten, *J. Phys. Chem. A* **113**, 184 (2009).
69. J. M. Ricart, M. P. Habas, A. Clotet, D. Curulla, F. Illas, *Surf. Sci.* **460**, 170 (2000).
70. B. L. Bhargava, S. Balasubramanian, *J. Phys. Chem. B* **111**, 4477 (2007).

APPENDIX A

EXPERIMENTAL PROTOCOL

A1. Making the Catalyst Ink For Electrochemical Cells

1. Weigh out 5.6mg of Pt black or Pt-Ru black into a scintillation vial.
2. Take a metered pipette and measure out 1ml of Millipore water
3. Make an ice bath
4. Sonicate the catalyst ink at the lowest frequency setting in the ice bath for 2 min
5. Take a metered pipette and deposit 2 aliquots of 25µl of the catalyst ink and deposit it on the gold support.
6. While the droplet is not flat, keep the electrode under a IR lamp connected to approximately 80V.
7. Once droplet begins to flatten, allow the ink to air dry for at least an hour.
8. Note that insufficient drying time, or leaving the droplet under the IR lamp for too long can cause catalyst to fall off during experiment
9. If catalyst continuously falls off, it may be necessary to reduce the catalyst ink under 400C Hydrogen gas (using BET) to reduce the oxides causing the poor adhesion.

A2. Making the Electrodes for the Flow Cell

1. Weigh out 10mg of Pt black or Ag nanopowder for cathode.
2. Weigh out 4mg of Pt black for anode.
3. For anode, cut out Ion Power carbon paper to size of reactor cross section
4. For cathode, cut out Ion Power carbon paper to a size just larger that gas channel cross section (approx 1.2cm x 2.2cm).
5. For either electrode, add 100µl of Millipore water
6. For either electrode, add 100µl of IPA. (Be sure to add water first!)
7. Add approximately 5.6µl of 5% Nafion.
8. Make ice bath
9. Sonicate catalyst ink at the lowest frequency setting in the ice bath for 2 min
10. Under an IR lamp (hooked up to approx 100V), with a detail brush, paint the entirety of the catalyst ink onto the carbon paper.
    a. For cathode, paint entirety of carbon paper
    b. For anode, paint in center approx 1cm x 2cm

A3. Cleaning Glassware

1. Take glassware and clean with Millipore water
2. Place glassware in a Nochromix Bath
    a. Norchromix bath is made by mixing ½ pkg. of Nochromix crystals and mixing with pure sulfuric acid in a glass container approx 100x190.
3. Allow to sit for at least 4 hours, overnight O.K.

4. Remove glass from Nochromix bath into a container with Millipore water to dilute excess sulfuric acid.
5. Diligently clean glassware in flowing Millipore water to remove all excess sulfuric acid.
6. Place glassware in an acid bath containing 50%/50% Nitric Acid and Millipore water.
7. Keep in nitric acid bath overnight
8. Remove glass from nitric acid bath into a container of Millipore water
9. Repeat step 5 (except to remove nitric acid)
10. Place glassware in boiling Millipore water for 1 hr
11. Remove glassware from boiling bath and place in oven (s.p. 125C) overnight.
12. Allow glass to cool.

A4. Electrode Polishing, Cleaning and Storage

1. All metal electrodes may be stored in 0.5-1M Sulfuric Acid in Millipore water.
2. Prior to depositing catalyst ink, polish electrodes using 1000/1500 grit paper with diamond colloid suspension (blue).
3. Make figure-8 motion both CW and CCW to keep uniformity in crystal exposure.
4. Wash with Millipore water
5. Place a few drops of Millipore water on the same paper and re-polish to remove excess organic solvent from diamond colloid.

A5. Working Electrode Assembly

1. Take a piece of wire (white insulation) and strip it approx 2” on both ends
2. Take one end of wire and thread it through the hole in the gold/platinum electrode.
3. Thread the other end of the wire through the bottom of the glass working electrode capillary to the top of male lure lock joint exposing the other end of the stripped wire.
4. Para-film the lure-lock end of the capillary as to prevent gas from escaping.
5. Slide the lure-lock end of the capillary through the teflon joint (with o-ring) appropriately as to fit the glass mouth the 3-electrode cell.

A6. Auxiliary (Counter) Electrode Assembly

1. Attach 25x25 platinum mesh to a piece of 0.25mm dia platinum wire
2. Pass the wire through the counter electrode glass joint with the #7 threads at the top.
3. Slide a red silicone septum over the platinum wire.
4. Slide Teflon bushing with #7 threads through the platinum wire
5. Secure the bushing to the glass joint.

A7. Reference Electrode Assembly

1. Take 1 pc. of heat shrink and place it over the tapered end of the reference electrode capillary.
2. Place 1 Vycor frit into the heat shrink package so it sits on the end of the capillary.
3. Take a heat gun so the plastic wrap shrinks and secures the frit to the capillary.
4. Cut off the excess heat shrink with a clean blade.
5. Prepare a solution of 0.1M TBAP and 0.01M silver nitrate in acetonitrile.
6. Place a small amount of this solution in the capillary and cover with parafilm.
7. Place a small amount of this solution in a scintillation vial and place the Vycor tip end of the electrode in the vial. This is to allow the silver/acetonitrile solution to diffuse into the frit to allow electrical connection between this RE and the cell.
8. Allow at least 2 hours.
9. Polish (with 1000/1500 grit paper) the silver wire attached to the teflon cap.
10. Wash silver wire with Millipore water
11. Place the teflon cap with the silver wire over the top end of the electrode making sure the silver wire is in contact with the silver/acetonitrile solution.

A8. Ferrocene Calibration and RHE Calibration

1. Measure out approximately 10-15ml of solvent into the electrochemical cell.
2. Depending on the volume of electrolyte added, add 2.5mM of Ferrocene into the electrochemical cell.
3. Prepare the platinum working, and counter electrode as well as the reference electrode as described above.
4. Scan the potential of the working electrode between -500mV and +500mV at 10mV/s.
5. If the full faradaic wave is not observed in this window, adjust the vertices accordingly until the full reversible faradaic wave is seen.
6. The formal potential can be taken as the midpoint between the peak oxidation and peak reduction potential.
7. For RHE Calibration, assemble the same electrodes, less the ferrocene, and bubble hydrogen over the counter electrode.
8. For RHE Calibration, measure the open circuit potential between the reference and the counter electrode.

A9. General CO_2 Reduction

1. Assemble the electrochemical cell by placing the counter electrode into the leftmost mouth of the customized electrochemical cell.

2. Place the working electrode assembly in the middle mouth of the customized electrochemical cell.
    a. Do not make contact with solution. Keep as high up as possible.
3. Cap off the rightmost mouth of the cell.
4. Place the lure-lock adapter for the sparger on the left sparging arm of the cell.
5. Attach an argon line (controlled through a rotameter) to the adapter.
6. Fill the electrochemical cell with approx 10ml of electrolyte so that the electrolyte lever rises above the luggin capillary sticking through into the main chamber.
7. Parafilm all junctions to reactor to prevent leaks.
8. Place reference electrode in the right arm of the cell and make sure the adapter is closed.
9. Attach lure lock adapter to overhead gas inlet.
10. Attach lure adapter to cell gas outlet.
11. Turn on argon at 200sccm and fix the 3-way valve so that gas only goes to over the electrolyte.
12. Slowly open the reference electrode adapter so that the head pressure pushes the electrolyte through the luggin capillary into the reference chamber. As soon as electrolyte is in contact with the frit, close the reference adapter.
13. Turn the 3-way valve so that inlet gas is now sparged through solution
14. Begin to bubble argon through the electrolyte at 150sccm for 2 hours.
15. Turn the 3-way valve so that 150sccm argon flows overhead.
16. Lower the working electrode so it forms a meniscus with the electrolyte.
17. Confirm OCP with the solatron.

18. Scan between 0V→-2V→0.5V→0V at 50mV/s as an inital test for 40 scans
    a. This serves to clean the electrode.
    b. Adjust verticies if necessary (i.e. smaller window due to solvent or electrode.)
19. If after 40 scans there is a clean double layer region and the CV's are reproducible, save the last scan as the blank (or do an additional scan)
20. If scans are not reproducible, continue to condition the electrode.
21. Sparge CO_2 into the cell for 30 minutes.
22. Repeat step 18 but for less scans.
23. Evidence of CO_2 conversion is found by regions of increased current and/or faradaic waves when overlaying the argon and CO_2 scans.

A10. General Reduced CO_2 Oxidation

1. Prepare electrochemical cell similarly to A8.
2. Sparge CO_2 into cell at 150sccm for 30 min.
3. Hold the potential of the working electrode at a reducing potential for the desired amount of time.
4. Do not loose electrical connection
5. Sweep potential forward from reduction potential to +1.5-2V at 5mV/s

A11. General CO Stripping

1. Prepare electrochemical cell similarly to A8.
2. Sparge Argon through cell and condition electrode similar to A8.
3. Condition electrode with 40 scans as described in A8.

4. After conditioning, bubble CO through solution for 10 minutes while holding potential of working electrode at -100 to -200 vs Ag/Ag+.
5. Switch sparging gas to Argon WHILE STILL MAINTAINING ELECTRICAL CONNECTION!
6. Perform a CV between the holding potential and +1.5V at a scan rate of 5mV/s.
7. The first scan should show CO stripping, while the second scan will not show a CO peak.
8. Integrate this peak and use the factor of 420uC/cm^2 to calculate surface area.

A12. Ionic liquid preparation

1. Place sufficient ionic liquid in a clean vacuum flask and seal
2. Place flask on heat/stir plate and turn on ~2 for heat and high value for stir
3. Leave ionic liquid under these conditions at least overnight
4. After preparation, close valve outside flask to be sure it is sealed from the atmosphere
5. If liquid sits more than a few days following preparation, repeat procedure beginning at step 1 to ensure well-prepared ionic liquid for experiments.

A13. SFG Protocol

1. Assemble the clean electrochemical cell

a. All Kel-F and glass parts are cleaned in acid bath overnight and then dried thoroughly
b. Care must be taken to keep all components clean during storage and also during assembly procedure

2. Clean platinum counter electrode by hydrogen flame
3. Assure that platinum electrode is clean and free of defect by visual inspection

Electrochemical methods

1. Prior to placing electrochemical cell in the BB-SFG chamber, run a few full scan potential cycles at 200 mV s^{-1} from -1.5 V to +1.5 V followed by 40-100 potential cycles at 200 mV s^{-1} from 0.5 V to -1 V in an argon-saturated ionic liquid
    a. When cycles stabilize, check for evidence of water and surface impurities
    b. If neither is present, it is safe to move on to next step
    c. If water is present in the ionic liquid, it must be removed from the electrochemical cell and replaced with dry, freshly prepared ionic liquid (therefore, it is always good to have some backup liquid already prepared before beginning spectroscopy experiments)
    d. If surface impurities are evident on the platinum crystal, it must be removed and polished and/or flame annealed.

2. Place electrochemical cell in BB-SFG chamber and begin bubbling carbon dioxide in the ionic liquid for 30 minutes
3. Scan fifteen potential cycles at 200 mV s^{-1} from ~0.5 to -1 V vs SHE to adsorb enough CO to observe a strong BB-SFG peak
4. Once the laser is aligned a variety of experiments can be performed
    a. CO can be stripped from the electrode surface by scanning the potential out to +1.5 V vs SHE (or by setting that potential for a few seconds)
    b. TLE can be performed at slow scan rates, such as 5 mV s^{-1} in order to combine spectroscopy with electrochemistry
    c.

Preventing laser-assisted desorption

1. The adsorbed CO exhibits strong laser assisted desorption, so the visible beam should be reduced to 2.5 μJ when probing CO to prevent this
2. The IR beam intensity can also be lowered if necessary
3. To determine the amount of laser-assisted desorption, align the laser and hold the electrode at open circuit potential
    a. If the signal decreases while held in one spot, the CO is probably desorbing
    b. If the signal regains intensity when the laser beam is moved and then decreases again, the CO is certainly desorbing
4. When probing other peaks, such as ionic liquid peaks, the visible power can be increased to 4.0 μJ without any laser assisted desorption

A14. Flow Cell Experimental Protocol

1. Prepare Electrodes as described in A2.
2. Make sure epoxy for gas and liquid channels are unclogged.
3. Place the gas channel upside down on the table.
4. Place a small amount of vacuum grease by the screw holes around the entire perimeter (inside the 'radius of the screw holes')
    a. Placing grease too close to channel will prevent electrical connection with the cathode.
5. Place a teflon layer (with screw holes and central holes slightly larger than gas channel) onto the aluminum gas channel and seal to the grease.
6. Place cathode (with catalyst facing upwards) onto the opening in the teflon layer. (This should form 1 layer, using the teflon to prevent to lateral escape of gas)
    a. Note grease should not interrupt the connection between the cathode and the aluminum layer.
7. Take the Teflon liquid channel and place vacuum grease on both sides on the equivalent cross sectional position as described in step 4.
8. Place the liquid channel on top of the cathode layer.
9. Place the anode (catalyst facing downwards) over the teflon layer, again ensuring a good seal with the vacuum grease.
10. Place a gas channel (w/o tubing) onto the assembly with gas channel opening facing you. (this will make detecting leaks hard if liquid can fill up the chamber, so we assemble with the opening facing outwards.

11. Place 2 layers of Teflon liquid channel on top of the aluminum gas channel you just placed on.
12. Insert screws through the 10 holes making sure the cell is aligned and has not lost compression.
    a. Wrap a piece of stripped wire around the top of one screw making sure the wire touches the bolt threads and not the teflon, this will act as the cathodic current collector.
13. Make sure screws have teflon tubing on them to prevent short circuit.
14. Use the multimeter to check resistance between each screw you place in and the anode side aluminum layer to ensure no screws are short circuiting the cell.
    a. If the resistance is in the MΩ, it is probably ok.
    b. Possible short in kΩ, definite short in Ω.
15. Use appropriately sized hypodermic needles to connect to liquid and gas channels.
    a. Use epoxy to connect tubing to the inlet end of the needle making sure not to form clogs.
16. Flow CO2 through an MFC at 2.5sccm.
17. Flow Electrolyte through syringe pump at 500µl/min
    a. With IL, may need 1ml/min to provide sufficient pressure.
18. Wrap cell with heating tape if necessary.
    a. You can get to 120C with approx 40V.
19. Insert another piece of wire in the hole of the bottom aluminum plate, this will act as the anodic current collector.

20. Once liquid and gas flow are confirmed, place the outlet liquid stream into a scintillation vial with a reference electrode.
21. Connect WE on the solatron to the WE, CE to CE, and cross RE1 and RE2 to be connected to the RE.
22. Measure OCP to ensure there is no short with liquid and gas flow.
23. Control potential between anode and cathode with potentiostat
24. Measure cathodic and anodic polarization WRT RE with 2 mulitmeters.
25. Run potentiostatically at ~2.25, 2.5, 3V (or desired level) for as long as needed.
26. Feed exit gas steam into GC

A15. Gas Chromatograph

1. Start flow of He to GC, set outlet pressure to 40psi
2. Turn on GC
3. Turn on Current to TCD to 125mA.
    a. Do not turn on current until you have confirmed carrier gas flow!
    b. If not confirmed flow, make sure injection port on front is sealed.
    c. Use Point Source TCD Leak Detective to find leaks within the oven column.
4. Set oven temp to 100C
5. Set TCD temp to 110C
6. Make sure TCD measures sufficient voltage.

    a. Make sure red, blue, green, black leads to wheatstone bridge of TCD are properly connected to their junctions
    b. This was jimmy-rigged outside of the GC on the right side.
7. Allow GC to warm up for at least an hour.
8. Rotate valve (G) at 0.1 min to allow aliquot of gas into column
    a. Moly Sieve 5A, 6'.
9. Watch for peaks, keeping in mind baseline drift with this particular column.
10. In the case where there is crossover in the cell, BE VERY CAREFUL NOT TO ALLOW LIQUID INTO THE INJECTION VALVE!

AUTHOR'S BIOGRAPHY

Brian Rosen was born and raised in Wilmington, Delaware. He went to high school at the Charter School of Wilmington and graduated with distinction in 2004. Brian received his Honors Bachelors in Chemical Engineering with Distinction from the University of Delaware in 2008. While at Delaware, Brian worked under Prof. Norman Wagner helping to develop liquid body armor (shear thickening fluid) for use in military, police, and correctional armor applications. Brian joined Richard Masel's research group at the University of Illinois in December 2008 and has been working on the low temperature and potential conversion of CO_2 to fuels.